Drosophila ELYS regulates Dorsal dynamics during development

Saurabh Jayesh Kumar Mehta[‡1], **Vimlesh Kumar**[§], and **Ram Kumar Mishra**[‡2]

From the ‡Nups and SUMO Biology Group, Department of Biological Sciences, and §Laboratory of Neurogenetics, Department of Biological Sciences, Academic Building 3, Indian Institute of Science Education and Research-Bhopal, Bhopal By-pass Road, Bhauri, Bhopal, Madhya Pradesh-462066, India

Edited by Phyllis I. Hanson

Embryonic large molecule derived from yolk sac (ELYS) is a constituent protein of nuclear pores. It initiates assembly of nuclear pore complexes into functional nuclear pores toward the end of mitosis. Using cellular, molecular, and genetic tools, including fluorescence and Electron microscopy, quantitative PCR, and RNAi-mediated depletion, we report here that the ELYS ortholog (*d*Elys) plays critical roles during *Drosophila* development. *d*Elys localized to the nuclear rim in interphase cells, but during mitosis it was absent from kinetochores and enveloped chromatin. We observed that RNAi-mediated *d*Elys depletion leads to aberrant development and, at the cellular level, to defects in the nuclear pore and nuclear lamina assembly. Further genetic analyses indicated that *d*Elys depletion re-activates the Dorsal (NF-κB) pathway during late larval stages. Re-activated Dorsal caused untimely expression of the Dorsal target genes in the post-embryonic stages. We also demonstrate that activated Dorsal triggers apoptosis during later developmental stages by up-regulating the pro-apoptotic genes *reaper* and *hid*. The apoptosis induced by Reaper and Hid was probably the underlying cause for developmental abnormalities observed upon *d*Elys depletion. Moreover, we noted that *d*Elys has conserved structural features, but contains a noncanonical AT-hook–like motif through which it strongly binds to DNA. Together, our results uncover a novel epistatic interaction that regulates Dorsal dynamics by *d*Elys during development.

The embryonic large molecule derived from yolk sac (ELYS)[3] was characterized in the mouse as a putative transcription fac-

tor important for hematopoiesis (1). ELYS was characterized to possess nuclear localization signal (NLS), nuclear export signal, N-terminal β-propeller region, central helical region, and C-terminally disordered region (1, 2). AT-hook motifs present in ELYS allow DNA binding, and the transactivation domains (acidic region) can induce transcription (1). The β-propeller–like domain present in ELYS mediates interaction with other nucleoporins and facilitates the nuclear pore complex (NPC) assembly (3). NPC is a multiprotein assembly of nucleoporins (Nups) with their sizes varying from ~60 MDa in yeast to ~125 MDa in metazoans. Nucleoporins assemble into subcomplexes and are present on the cytoplasmic, nuclear membrane, and nucleoplasmic faces of nuclear pores (4, 5). In metazoans, at the onset of mitosis, subcomplexes of NPCs dissociate from each other and get redistributed inside the cell. ELYS was reported to be an integral member of the Nup107 complex and essential for post-mitotic NPC assembly (6–10). In interphase, ELYS is present at the nuclear envelope and nucleoplasm, but in mitosis, it associates with chromatin, kinetochores, and spindles (8). Importantly, the conserved ELYS domain is required for its NPC and kinetochore localization (11), where ELYS helps in microtubule polymerization (12). ELYS tethers Nup107 complex to kinetochores and initiates their inclusion into post-mitotic nuclear pores (9).

ELYS is critically required for embryonic development as *ELYS* null mice die during embryonic stage E3.5 to E5.5, well before the onset of embryonic hematopoiesis (1, 13). However, conditional inactivation of the *ELYS* locus in adult mice showed reduced effects, and mice behaved normally (14). ELYS, also known as Mel-28, is required for the maintenance of the nuclear morphology and embryonic development in *Caenorhabditis elegans* (7, 10). The ELYS ortholog in zebrafish, *flotte lotte* (*flo*), is critically required for early embryonic and pharyngeal skeleton development (15). Additionally, *flo* deletion disrupted NPC formation, and defective nuclear import induced replication stress in intestinal progenitor cells (16).

In addition to the NPC assembly, the depletion of ELYS leads to phosphorylation-dependent mislocalization of lamin B receptor (LBR) from the nuclear periphery (17). ELYS recruits protein phosphatase-1 (PP1) to the kinetochores, and a reduction in phosphorylation levels of various molecules drives

interest; oligo, oligonucleotide; FISH, fluorescence *in situ* hybridization; SEM, scanning electron microscopy; DGRC, *Drosophila* Genomics Resource Centre.
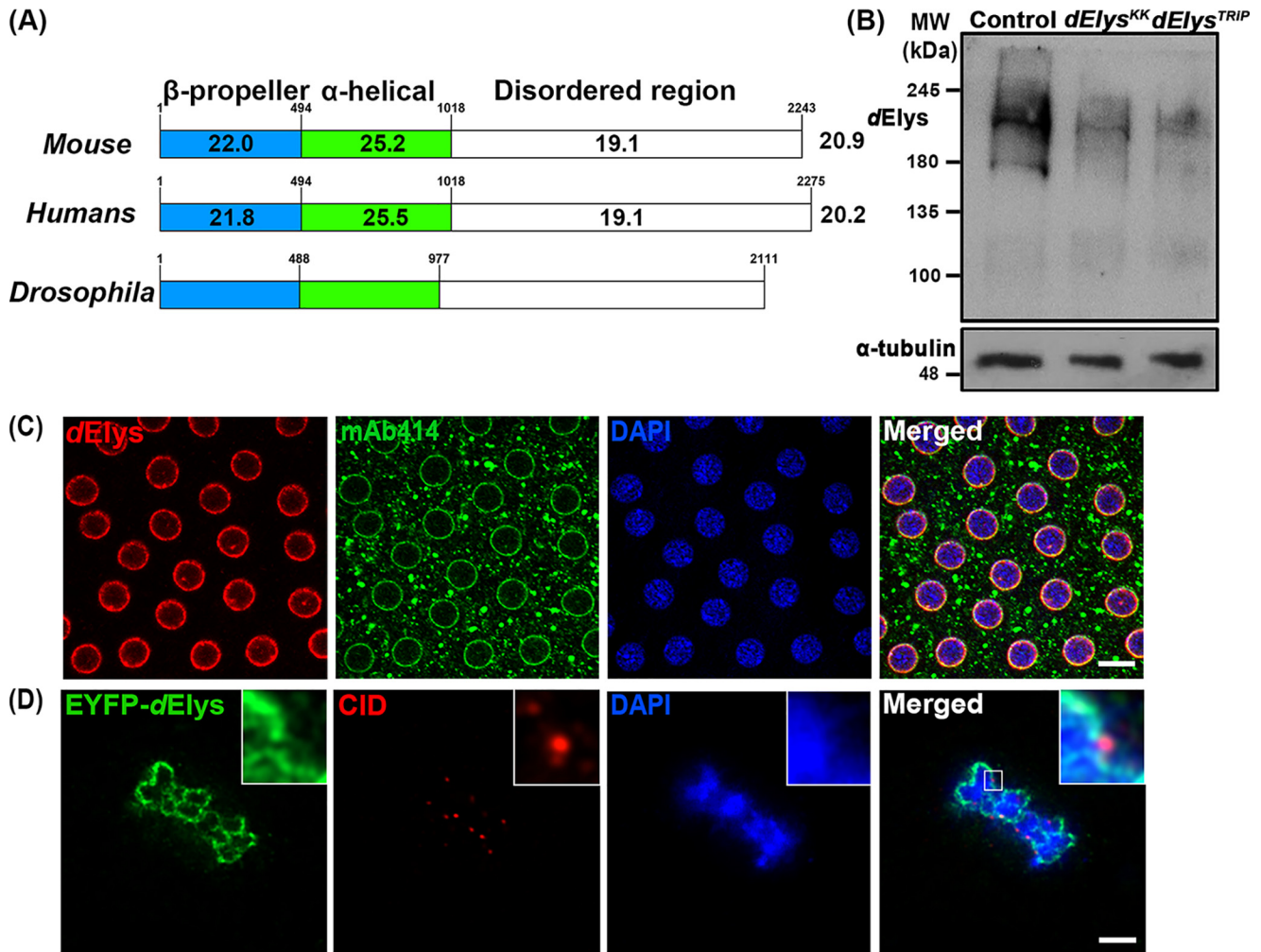
Figure 1. ELYS is conserved in *Drosophila*. *A,* graphical representation of sequence identity of *d*Elys with mouse and human ELYS. *d*Elys is 20.9 and 20.2% identical with mouse and human ELYS, respectively. Domain-wise identity is mentioned in each domain. Conserved secondary structures between *Drosophila*, mouse, and human ELYS are represented. β-Propeller N-terminal domain, α-helical central domain, and disordered C-terminal regions are conserved in *d*Elys as in higher orthologs. *B,* antibody generated against *d*Elys identified a band of ∼215 kDa in lysates obtained from third instar larval head complex from WT control and ubiquitous *d*Elys knockdown lines as indicated. α-Tubulin was used as a loading control. *C,* syncytial *Drosophila* embryos stained with *d*Elys antibody (*red*), mAb414 (*green*) marking FG-nucleoporins, and DNA stained with DAPI. *Scale bar,* 5 μm. *D,* high-resolution image of metaphase-arrested *Drosophila* S2-expressing EYFP–tagged *d*Elys (*green*) stained for kinetochores with an anti-CID antibody (*red*). *Scale bar,* 2 μm.

nuclear envelope assembly (18). Thus, ELYS being a nucleoporin and putative transcription factor is a critical molecule that may have a significant role to play in the early developmental events of an organism. However, no directed study has been performed on ELYS to obtain mechanistic insight of important roles played by ELYS in cellular homeostasis and early developmental events.

We chose *Drosophila melanogaster* (fruit flies) to address the importance of ELYS in early developmental processes. CG14215, an ELYS-like molecule in *Drosophila* (hereafter as *d*Elys), is known to be present at the nuclear periphery and in association with the promoter region of genes undergoing active transcription (19, 20). Here, we report the genetic, molecular, and cellular characterization of *d*Elys. *d*Elys binds with DNA through its noncanonical AT-hook–like motif. RNAi-mediated depletion of *d*Elys induces loss of nucleoporins and lamins, thus affecting the nuclear pore and nuclear lamina assembly. Importantly, upon *d*Elys depletion, Dorsal (NF-κB) accumulates inside the nucleus in later larval

stages, without any immune challenge, and induces apoptosis. Through our results, we strongly imply that *d*Elys is a key developmental molecule required in cellular processes integral to normal cellular homeostasis. In addition to maintaining the nuclear architecture, *d*Elys contributes to the development by regulation of the Dorsal dynamics into post-embryonic tissues.

Results

ELYS is highly conserved in Drosophila

ELYS is a DNA-binding nucleoporin that coordinates NPC assembly at the end of mitosis. *Drosophila* ELYS (*dElys*, CG14215) is known to localize at the nuclear periphery and is found to be present at the promoter region of genes undergoing active transcription (19, 20). However, any mechanistic details on the *d*Elys function are not available. For molecular and cellular characterization of *d*Elys, we started with primary sequence alignment and report that an overall ∼20–21% identity exists among *d*Elys and mouse and human ELYS (Fig. 1*A*).

Using bioinformatics tools, we have predicted the presence and conserved arrangement of structural features like the N-terminal β-propeller domain (aa 1–488), central helical domain (aa 489–977), and a C-terminal unstructured region (Fig. 1A). Homology-based 3D structure predictions of the N-terminal β-propeller domain of *d*Elys identified a highly-conserved seven-bladed β-propeller structure (Fig. S1A) appreciably similar to the reported structure of the N-terminal domain of mouse ELYS (3, 21). Evolutionary divergence analysis indicates that *d*Elys is present in a clade quite distinct and distant from vertebrate ELYS (Fig. S1B).

We raised polyclonal antibodies against the C-terminal antigenic fragment (aa 1796–2111) of *d*Elys. Immunoblotting with anti-*d*Elys antibody detected a band of ~215 kDa in control head complex lysates and a band of decreased intensity in lysates prepared from tissues where *d*Elys was ubiquitously knocked down (ubiquitous knockdown was achieved by driving *d*Elys RNAi with the *Act*5C–GAL4 driver, to be denoted as ubiquitous here on) (Fig. 1B). *d*Elys antibodies detected a conserved and strong nuclear rim staining pattern in syncytial embryos overlapping with mAb414 antibodies recognizing FG-nucleoporins in nuclear pores (Fig. 1C). *d*Elys antibodies also detected a similar overlapping pattern at the nuclear rim of salivary gland nuclei from GFP–Nup107-expressing organisms (Fig. S1C). Moreover, the EYFP–*d*Elys-expressing salivary glands also had a nuclear rim localization pattern identical to endogenous *d*Elys (Fig. S1D). In salivary gland nuclei, *d*Elys antibodies detect a pattern co-localizing with the nuclear lamina–associated lamin-B receptor at the nuclear periphery (Fig. S1E). We probed whether *d*Elys also exhibits cell-cycle–dependent subcellular localization changes as seen in other organisms. Metaphase-arrested EYFP–*d*Elys-expressing *Drosophila* S2 cells were co-stained with the centromere identifier (CID, *Drosophila* CENP-A homolog) (22) to mark the kinetochores. *d*Elys localized to mitotic chromosomes but not on the kinetochores. Rather, *d*Elys was observed in the close vicinity of CID puncta. It is important to note that ELYS recruits the Nup107 complex to the kinetochores in cell culture, *Xenopus* egg extracts, and *C. elegans* embryos (6–8, 12). However, the Nup107 complex was reported to be absent from kinetochores in *Drosophila* (23).

ELYS is also known as an AT-hook–containing transcription factor 1 (AHCTF1). Using a canonical mouse ELYS AT-hook motif (*Mm*_Elys_AT-hook), we have predicted three AT-hook–like motifs in *d*Elys. We noticed a lack of glycine and proline amino acids in the conserved –RGRP– core (overscored) present in several characterized AT-hook proteins (Fig. S2A) (24). We thus asked whether such a divergent noncanonical AT-hook can bind DNA. A C-terminal fragment (aa 1858–1961) of *d*Elys bearing all three predicted AT-hook–like motifs, *d*Elys_AT-1, -2, and -3, was purified and tested in a DNA-binding assay. Together with this, we mutated the arginines in each predicted AT-hook–like motif individually (mAT-1, mAT-2, and mAT-3, where "m" denotes arginines of the AT-hook mutated to alanines) or combined the mutations of all three AT-hooks (mAT-1 + 2 + 3) (Fig. S2B) and tested the ability of purified proteins (Fig. S2C) to bind with AT-rich or non-AT–rich DNA. It is evident from the EMSA experiments and their

quantitation that mutations in AT-hook 1 and 3 (mAT-1 and mAT-3) show a significant reduction in their ability to bind with both AT-rich and non-AT–rich DNA (Fig. S2, D–G). Our data further established that the presence of glycine and proline is not as important in the –RGRP– core as the positively charged arginine. The alternately placed positively charged amino acids are known to play more important role in AT-hook functions (25). Through our initial *in silico*, biochemical, and cellular analysis, we suggest that *d*Elys is a canonical ELYS molecule despite low sequence identity.
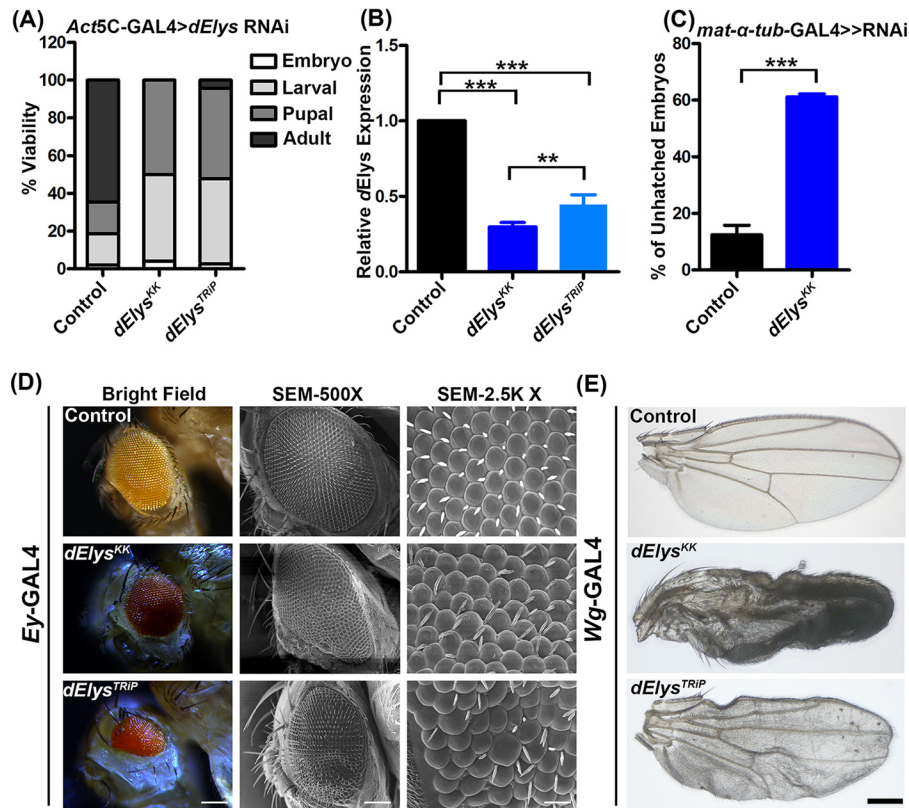
*d*Elys is essential for normal development in *Drosophila*

After assigning features of a nucleoporin and determining the localization dynamics, we asked whether *d*Elys is essential for development in *Drosophila*. We performed *in vivo* depletion of *d*Elys using RNAi line (v103547) from the Vienna *Drosophila* Resource Centre (VDRC) (*d*Elys^{KK}). To validate phenotypes observed with the *d*Elys^{KK} RNAi line, we also generated a TRiP-based RNAi line (*d*Elys^{TRiP}). The ubiquitous knockdown of *d*Elys by the two RNAi lines led to severe consequences on viability and induced lethality with a varying extent at each developmental stage. Although no adults emerged from the *d*Elys^{KK} RNAi line, a few viable flies (~4%) emerged out in *d*Elys^{TRiP}. *d*Elys-depleted embryos were largely unaffected (~4% lethality), but a significantly increased lethality occurred at the larval stage (~46%), and ~50% of pupae died in the late pupal stage of development (Fig. 2A). The quantitative PCR-based assessment of knockdown in *d*Elys transcript levels suggests ~70 and ~55% knockdown in *d*Elys^{KK} and *d*Elys^{TRiP} RNAi lines, respectively (Fig. 2B). Although *d*Elys^{KK} has two predicted off-targets, *CG15643* and *CG7051*, in addition to *d*Elys, the expression level of *CG15643* remained unperturbed, while the *CG7051* levels decreased by ~20% during *d*Elys knockdown ($p < 0.05$) (Fig. S3, A and B). *CG7051* is reported to have an exclusive expression in male germ cells (26) and hence would not have contributed to the phenotypes observed. We have used the *d*Elys^{KK} line in all subsequent studies because it showed a comparatively significant knockdown, and the pVALIUM10-based TRiP line is relatively ineffective in knockdown during oogenesis as well as a lack of uniform knockdown (27).

Maternally contributed *d*Elys will hinder the analysis for developing an understanding of *d*Elys functions in early development. We thus used the *mat–α-tub*–GAL4 driver to deplete maternally contributed *d*Elys before the induction of zygotic transcription to overcome this issue. Maternally depleted *d*Elys (*d*Elys^{KK} RNAi line) embryos have an abnormal shape, and they show a very slow rate of development compared with control embryos (data not shown). Hatching rate analysis showed that maternal *d*Elys-depleted embryos showed ~62% lethality as compared with ~12% lethality observed with control embryos obtained by crossing control flies with the driver line (Fig. 2C).

To avail more insights on the importance of *d*Elys in development, we silenced *d*Elys in a tissue-specific manner in eyes and wings using eyeless (*Ey*) and wingless (*Wg*) drivers, respectively. *d*Elys-depleted flies have a shrunken eye with a significant reduction in the area occupied by ommatidia. Also, the ommatidia shape was irregular, and their arrangement was in disarray, leaving behind an eye cavity (Fig. 2D, *1st and 2nd*

Figure 2. *d*Elys is essential for the normal development of *Drosophila*. *A,* quantification representing the lethality stages of the *dElys* knockdown organism. RNAi lines were driven with ubiquitous *Act*5C–GAL4 driver. Control represents WT flies crossed with the *Act*5C–GAL4 driver. *B,* quantitative PCR for *dElys* knockdown using two different RNAi lines. Data are represented from at least three independent experiments. Statistical significance was derived from one-way ANOVA followed by Tukey's post hoc test. *Error bars* represent S.E. *** represents $p < 0.0001$, and ** represents $p < 0.001$. *C,* hatching rate analysis of maternal depletion of control and *dElys* in embryos using *mat-α-tub*-GAL4 ≫ RNAi driver. *D,* eye-specific knockdown of *dElys* using the *Ey*-GAL4 drivers. The *1st column* shows the stereomicroscopic image; the *2nd column* represents the SEM image (×500), and the *3rd column* shows an SEM image (×2.5K). Observations were made from at least three independent experiments. *Scale bar,* 200 μm in the stereomicroscopic image; 20 μm in SEM *column 1*, and 2 μm in SEM *column 3*). *Control* represents WT flies crossed with *Ey*-GAL4 driver. *E, dElys* depletion in the wing using the *Wg*-GAL4 driver. Representative images are shown for wing phenotypes. Observations were made from at least three independent experiments. *Scale bar,* 200 μm. *Control* is WT flies crossed with *Wg*-GAL4driver.

vertical panels). Moreover, a significant number of *dElys*-depleted ommatidia show loss of eye bristles, duplication of bristles, and an irregular orientation (Fig. 2*D, 3rd vertical panel*, SEM ×2.5K). Similarly, *dElys*-silenced wings look crumpled with signs of vein atrophy and significant cell death in the wing blade tissues (Fig. 2*E*). The severity of these phenotypes varied between the two different *dElys* RNAi lines used in this study, yet the observations made regarding eye and wing phenotypes were consistent. Our data thus suggest an essential requirement of *d*Elys for the normal development of *Drosophila*.

Loss of dElys results in the nuclear pore and nuclear lamina assembly defects

We next asked whether the *d*Elys is functionally conserved in *Drosophila*. We assessed the localization of various nucleoporins representing different subcomplexes of NPC when *dElys* is ubiquitously knocked down. When salivary gland nuclei from *dElys* knockdown flies were stained for Nup43, representing the Nup107 complex, Nup98, a mobile nucleoporin (Fig. S4, *A* and *B*), and mAb414 antibody recognizing FG-repeats, they were found to be largely absent from the nuclear membrane (Fig. 3, *A* and *B*, *right panels*). Concomitantly, a marked increase in the cytoplasmic staining for these nucleoporins was observed in the *dElys*-depleted salivary gland tissues indicating a redistribution

of nucleoporins. Quantitation of nuclear membrane intensities for different Nups also corroborates the fact that *d*Elys affects efficient assembly of nucleoporins into NPC (*d*Elys: control, 1.00 ± 0.04, and *dElys^{KK}*, 0.15 ± 0.01; Nup43: control, 1.00 ± 0.08, and *dElys^{KK}*, 0.29 ± 0.02; Nup98: control, 1.07 ± 0.12, and *dElys^{KK}*, 0.31 ± 0.02; FG-repeat nucleoporins: control, 1.00 ± 0.07, and *dElys^{KK}*, 0.36 ± 0.01) (Fig. S4, *G–J*). We have further confirmed with histone H3 staining that *dElys* depletion does not alter chromatin structure significantly (histone H3: control, 1.00 ± 0.06, and *dElys^{KK}*, 0.85 ± 0.03) (Fig. 3*D*) and hence could be used for normalization of intensities of every molecule tested. Detection of the protein levels of these nucleoporins in the larval head– complex lysate suggests no significant decrease in their levels except for Nup98 (Fig. 3*E* and Fig. S4*P*). Our data thus establish a conserved role for *d*Elys in post-mitotic NPC assembly in *Drosophila*.

ELYS regulates the incorporation of LBR in the nuclear envelope in a phosphorylation-dependent manner (17, 28). So, we asked whether the nuclear lamina assembly is also affected by *d*Elys. Salivary gland tissues, ubiquitously depleted for *dElys*, when stained for lamin B, LBR, and lamin C showed reduced localization in the nuclear lamina (Fig. S4, *C* and *D*, and Fig. 3*C*, respectively). Quantitation of nuclear lamina intensities for lamina-associated molecules suggests a clear decrease under
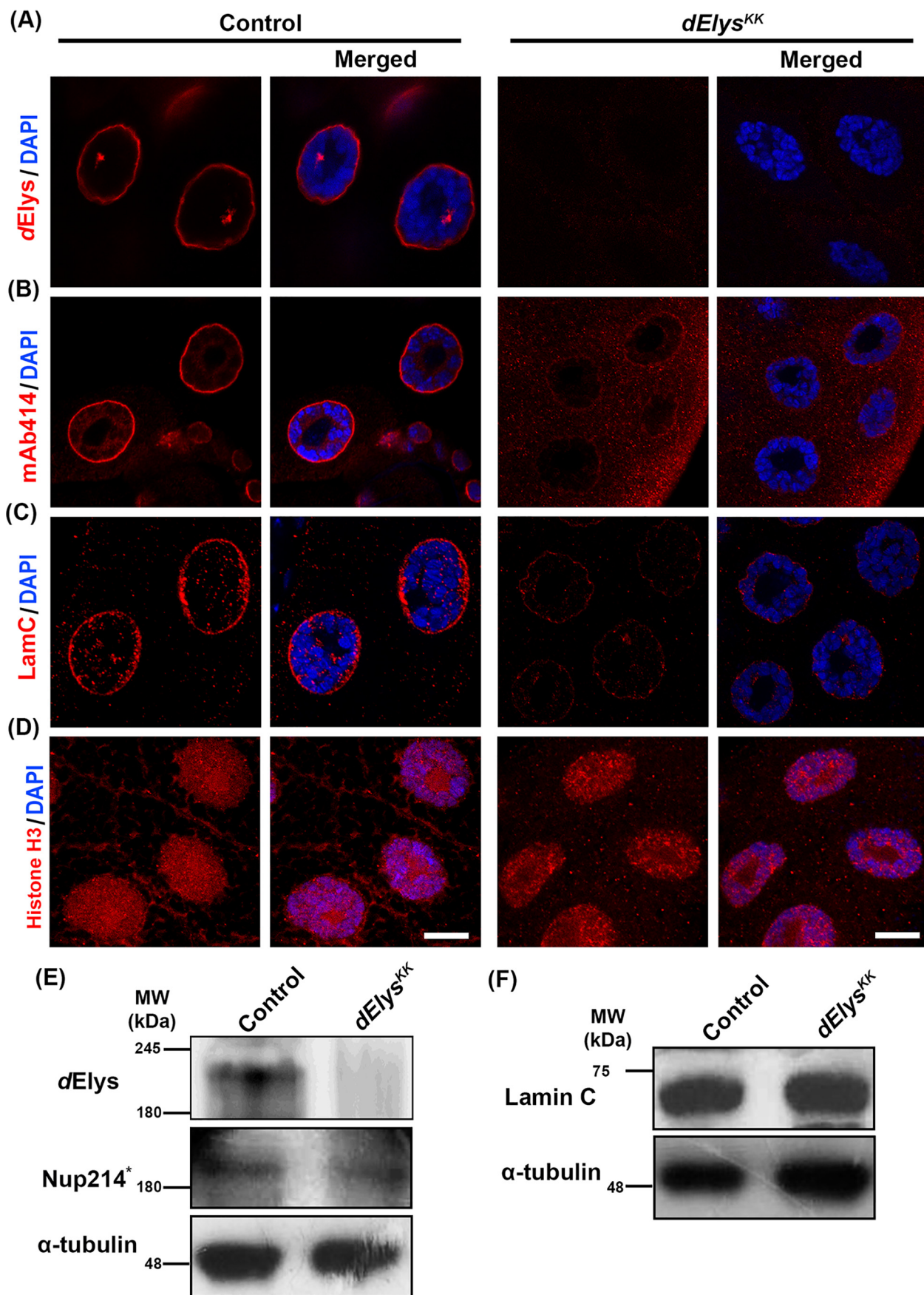
*d*Elys-depleted conditions, which emphasizes the importance of *d*Elys in the recruitment of these molecules to the nuclear lamina (LBR: control, 1.02 ± 0.07, and $dElys^{KK}$, 0.28 ± 0.01; lamin B: control, 0.98 ± 0.04, and $dElys^{KK}$, 0.50 ± 0.04; lamin C: control, 0.99 ± 0.04, and $dElys^{KK}$, 0.43 ± 0.01). Our data constitute the first report highlighting the *in vivo* importance of *d*Elys in the localization of lamin B and lamin C to the nuclear lamina. It is also important to note that during the *d*Elys depletion experiments, protein levels of lamins and LBR remained unaffected (Fig. 3*F* and Fig. S4*Q*). These observations suggested that *d*Elys is indispensable for the maintenance of the nuclear lamina and ultimately the nuclear architecture.

While analyzing the nuclear periphery localization of nucleoporins and lamins, we noticed that the Ran-GTPase, required for the coordination of the nucleo-cytoplasmic transport of protein cargo, is mislocalized upon *d*Elys depletion. In *d*Elys-depleted salivary gland tissues, Ran reactivity was lacking from the nuclear periphery and appeared redistributed throughout the cell (Ran: control, 1.03 ± 0.09, and $dElys^{KK}$, 0.29 ± 0.05) (Fig. S4, *E* and *N*). Upon *d*Elys knockdown, the absence of Ran-GTPase, Nups, and lamins prompted us to ask whether everything associated with the nuclear periphery is re-distributed. TBP-associated factors that form TFIID show nuclear rim and strong cytoplasmic staining in the *Drosophila* embryo (29). Accordingly, TATA-box binding protein-1 (TBP1, *d*TBP in *Drosophila*) when stained with polyclonal anti-yeast TBP antibodies (as used in Ref. 30) presented the characteristic nuclear periphery staining pattern even in the *d*Elys-depleted salivary gland tissues (*d*TBP: control, 1.00 ± 0.11, and $dElys^{KK}$, 0.76 ± 0.12) (Fig. S4, *F* and *O*). Unaltered protein levels of these molecules indicate that *d*Elys is required for their recruitment to the nuclear envelope, possibly during post-mitotic nuclear buildup where *d*Elys is the first molecule associating with DNA. A similar loss of FG-nucleoporins from the nuclear rim was noticed in salivary glands when *d*Elys was knocked down using a TRiP-based RNAi line (Fig. S5*A*, *bottom-most panels*). To further confirm the *d*Elys function in NPC assembly, we attempted to rescue *d*Elys depletion phenotype by multiple gene copy approach, where we provided an extra copy of *d*Elys (*UAS–dElys*) through a transgene to exhaust the dsRNA generated by RNAi (*dElys^{KK}*), leaving behind a significant amount of *d*Elys to perform its function. The FG-repeat nucleoporins analyzed in this combination (*dElys^{KK}; UAS-dElys*) showed partial rescue of its level on the nuclear periphery (FG-repeat nucleoporins: control, 1.00 ± 0.13; $dElys^{KK}$, 0.43 ± 0.01; $dElys^{KK}$; *UAS-dElys*, 0.71 ± 0.03) (Fig. S5*A*, *3rd horizontal panel, and B*), suggesting that the phenotypes observed were indeed a result of *d*Elys depletion.

*d*Elys knockdown shows activated Dorsal pathway and induced apoptosis

To deduce the underlying molecular mechanism that drives *d*Elys depletion phenotypes, we sought to check for perturbed nucleo-cytoplasmic traffic of various signaling molecules. Dorsal (NF-κB) is an important transcription factor, which stably associates with Cactus and remains inactive in the cytoplasm under normal conditions. The rapid shuttling of Dorsal into the nucleus requires a stimulus (31, 32) and is accompanied by ubiquitination-dependent degradation of the Cactus, NF-κB inhibitor (IκB) in the cytoplasm (33, 34). In salivary glands isolated from ubiquitous knockdown of control, the Dorsal signal was predominantly diffused in the cytoplasm (Fig. 4*A*, *upper panels*). In contrast, *d*Elys-depleted salivary gland tissues showed an intense Dorsal signal inside the nucleus (Fig. 4*A*, *lower panels*). Ratiometric quantification of the Dorsal intensities in the cytoplasm and nucleus further highlighted that Dorsal signals significantly increased inside the nucleus upon *d*Elys depletion (nuclear/cytoplasmic Dorsal: control, 1.00 ± 0.07, and $dElys^{KK}$, 4.93 ± 0.20) (Fig. 4*D*). Increased nuclear localization of Dorsal was also seen in salivary glands obtained from *d*Elys knockdown using the TRiP-based RNAi line (Fig. S5*C*, *4th horizontal panel*). Upon *d*Elys depletion, the increased retention of Dorsal inside the nucleus is not accompanied by an increase in *dorsal* transcript levels (Fig. S6*A*). Thus, *d*Elys regulates the redistribution of Dorsal, but not its expression. The accumulation of Dorsal inside the nucleus prompted us to ask whether the cytoplasmic level of Cactus has been reduced. The cytoplasmic Cactus signal is significantly diminished in *d*Elys-depleted salivary gland tissues as compared with control tissues (Fig. 4*B*). The quantification of Cactus staining further corroborated the observation that *d*Elys depletion may induce Cactus degradation and Dorsal accumulation inside the nucleus (Cactus: control, 1.00 ± 0.03, and $dElys^{KK}$, 0.40 ± 0.01) (Fig. 4*E*). Our attempts to rescue Dorsal nuclear localization by providing an extra copy of *d*Elys using transgene (*UAS–dElys*) led to Dorsal receding from the nuclei of the third instar larval salivary glands, suggesting a specific role of *d*Elys in nuclear Dorsal localization (nuclear/cytoplasmic Dorsal: control, 1.00 ± 0.07, and $dElys^{KK}$, 7.03 ± 0.47; $dElys^{KK}$; *UAS-dElys*, 1.33 ± 0.05) (Fig. S5, *C, 3rd horizontal panel, and D*). Although Dorsal is known to be a pro-growth molecule, studies suggest that activated Dorsal can also induce apoptosis in cells (35–37). The phenotypes observed upon *d*Elys depletion may be a consequence of the unfavorable accumulation of Dorsal inside the nucleus and thus could induce cell death.

We next probed whether the abnormal development of the eye and wing tissues, as well as lethality observed upon *d*Elys

Figure 3. *d*Elys is essential for the nuclear pore complex and nuclear lamina assembly in *Drosophila*. *A* and *B*, detection of *d*Elys (*A*) and FG-repeat nucleoporins (detected by mAb414, *B*) on the nuclear rim assessed in third instar larval control, (*1st* and *2nd vertical panels*) and *d*Elys-depleted (ubiquitous *Act*5C–GAL4 driven, *3rd* and *4th vertical panels*) salivary gland nuclei. DNA is stained with DAPI. *Scale bar*, 5 μm. *Control* is WT flies crossed with the *Act*5C–GAL4 driver. *C*, assessment of lamin C localization in third instar larval control, and *d*Elys-depleted (ubiquitous *Act*5C–GAL4 driven) salivary gland nuclei as mentioned in *A* and *B*. *Scale bar*, 5 μm. *D*, representative images of histone H3 (*red*) staining in control and *d*Elys-depleted (ubiquitous *Act*5C–GAL4-driven) third instar larval salivary gland nuclei. DNA is stained with DAPI. *Scale bar*, 5 μm. Control is WT flies crossed with the *Act*5C–GAL4 driver. *E*, Western blot analysis of indicated molecules tested in control and *d*Elys knockdown (ubiquitous *Act*5C–GAL4 – driven) third instar larval head lysate. * indicates detection with mAb414 antibodies. α-Tubulin was used as a loading control. *Control* is WT flies crossed with the *Act*5C–GAL4 driver. Each Western blotting was performed at least three times. *F*, Western blot analysis for nuclear lamina molecule lamin C as done in *E*. α-Tubulin was used as a loading control. Stripes separated from the same experiment were probed with additional antibodies as mentioned in Fig. S4P.
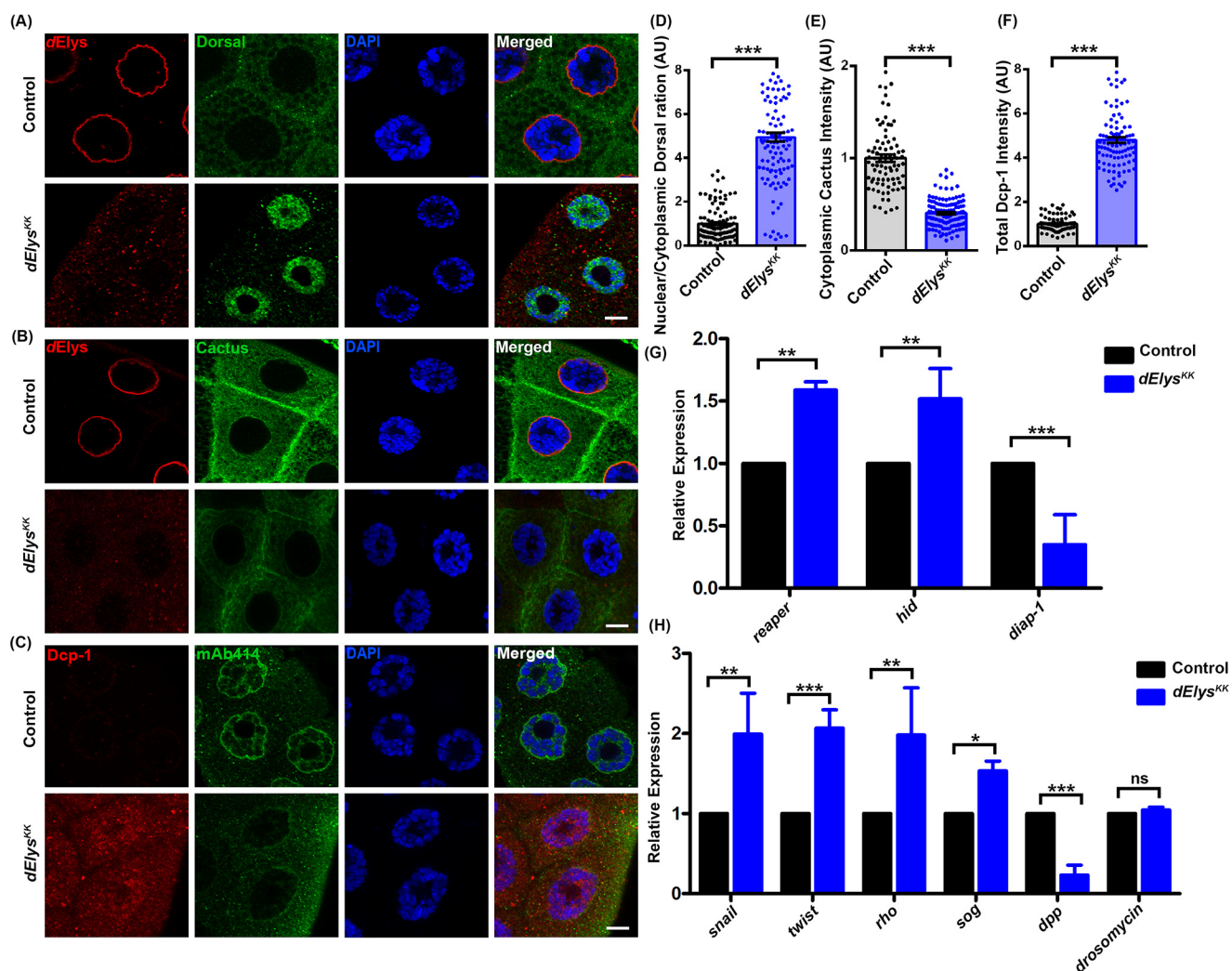
Figure 4. Dorsal is activated in *dElys* depletion and shows induced apoptotic response. *A*, detection of Dorsal with anti-Dorsal (*green*) and *d*Elys antibodies (*red*) in control (*upper panels*) and *dElys* RNAi (ubiquitous *Act*5C–GAL4 driven, *lower panels*) third instar larval salivary gland nuclei. DNA is stained with DAPI. *Scale bar*, 5 μm. *Control* is WT flies crossed with the *Act*5C–GAL4 driver. *B*, detection of Cactus in third instar larval salivary gland cells with anti-Cactus (*green*) as mentioned in *A*. *Scale bar*, 5 μm. *C*, detection of apoptosis in third instar larval salivary gland cells with anti-*Drosophila* caspase-1 antibody (*red*) and FG-nucleoporins by mAb414 antibodies in control (*upper panels*) and *dElys* depletion (ubiquitous *Act*5C–GAL4 driven, *lower panels*). DNA is stained with DAPI. *Scale bar*, 5 μm. Control is WT flies crossed with the *Act*5C–GAL4 driver. *D–F*, quantification of intensities of indicated molecules in control and *dElys* RNAi condition. The intensity of each molecule was normalized to the intensity of DAPI. Data are represented from at least three independent experiments. At least 45 nuclei were analyzed from 7 to 8 pairs of salivary glands. Statistical significance was derived from the Student's *t* test. *Error bars* represent S.E. *** represents $p < 0.0001$. *G*, expression analysis of apoptosis regulatory genes, *reaper*, *hid*, and *diap-1* by quantitative PCR in cDNA from third instar larval head complex of control and *dElys* RNAi (ubiquitous *Act*5C–GAL4 driven). Data are represented from at least three independent experiments. Statistical significance was derived from the Student's *t* test. The *error bars* represent the standard deviation. *** represents $p < 0.0001$, and ** represents $p < 0.001$. *H*, expressions of Dorsal target genes *snail*, *twist*, *rho*, *dpp*, short gastrulation (*sog*), and drosomycin analyzed by quantitative PCR in control and *dElys* RNAi (ubiquitous *Act*5C–GAL4 driven) third instar larval head complex lysate. Data are represented from at least three independent experiments. Statistical significance was derived from the Student's *t* test. The *error bars* represent the standard deviation. *** represents $p < 0.0001$, and ** represents $p < 0.001$, and * represents $p < 0.05$; *ns* is nonsignificant.

depletion, is due to apoptosis. We employed acridine orange staining as a primary assay to infer the induction of apoptosis in salivary glands. *dElys*-depleted tissues accumulated significantly more acridine orange than normal tissues suggesting activation of cell death (data not shown). To further assert whether *dElys* depletion can induce cell death (apoptotic response), we probed for cleaved Death caspase-1 (Dcp-1). Dcp-1 is critical for normal embryonic development, and an elevation in Dcp-1 levels is a hallmark for apoptosis (38 –40). Dcp-1 staining of salivary gland tissues from ubiquitous *dElys* knockdown showed increased immunoreactivity and increased Dcp-1 positive puncta (cleaved Dcp-1: control, 1.00 ± 0.03, and

dElys^{KK}, 4.79 ± 0.13) (Fig. 4, *C* and *F*). We next asked whether nuclearly-accumulated Dorsal causes any alterations in the expression of apoptotic genes. We probed for the transcript levels of pro-apoptotic genes *reaper* and *hid* and anti-apoptotic *diap-1* (*Drosophila* inhibitor of apoptosis 1). cDNA was prepared from the third instar larval head complex isolated from the ubiquitous knockdown of control and *dElys*, and the transcript levels were assessed by quantitative real-time PCR. We observed a significant increase in the level of the pro-apoptotic *reaper* and *hid* expression, although there was a complementary decrease in the level of anti-apoptotic *diap-1* upon *dElys* depletion (Fig. 4*G*). The relative levels of *diap-1*, *reaper*, and *hid*

are important determinants of cell survival or cell death. Together, the quantitative PCR and Dcp-1 immunostaining data indicate an indisputable correlation toward apoptotic induction upon *dElys* depletion. Accumulation of Dorsal upon *dElys* knockdown should bring a change in the levels of its target genes. The quantitative PCR-based detection of *snail*, *twist*, *rho*, and *sog* levels revealed an increase in their expression. However, the levels of *dpp* (decapentaplegic), a gene suppressed by Dorsal, decreased in *dElys*-depleted samples as compared with control (Fig. 4*H*). To rule out the possibility of an activated Dorsal pathway under immune response, we checked for the expression of the anti-microbial peptide drosomycin in *dElys*-depleted cDNA. The unaltered *drosomycin* levels suggest that *dElys* depletion-dependent activation of the Dorsal pathway does not have a microbial infection and immunity component to it (Fig. 4*H*).

Dorsal-dependent expression of *snail*, *twist*, and *sog* during early development is important for cellularization (41). We used the third instar larval head complex for cDNA preparation, which is quite late in the development. Expression of *snail*, *twist*, and *sog* could be detected in the late larval stages and that may be the cause of apoptosis in *dElys*-depleted organisms inducing developmental defects. Studies indicate that *Drosophila* apoptotic response activators include *snail*, *twist*, *dpp*, and *rho* (42–45). It is thus not surprising to find resurrected expression of Dorsal targets during late developmental stages that could induce apoptosis and developmental defects observed under *dElys*-depleted conditions.

Accumulation and re-activation of Dorsal in post-embryonic tissues is dElys specific

We set out to investigate whether *dElys* depletion-dependent nuclear retention of Dorsal is a temporal event of later developmental stages or whether Dorsal is entrapped in the nucleus even after the embryonic stage. First, we analyzed the Dorsal levels in early embryonic stages (stage 5) in control and *dElys* knockdown were driven by $mat-\alpha-tub$–GAL4. The nuclear levels of Dorsal remain high and unperturbed in both *dElys* and control-depleted embryos (Fig. 5*A*, *1st vertical panel*). Significant nuclear Dorsal levels along with increased cytoplasmic localization of Dorsal was observed in presumptive embryonic salivary glands from late embryonic stages (stage 15) of control and *dElys*^{KK} organisms (Fig. 5*A*, *2nd vertical panel*). We then looked for Dorsal signals in the nuclei of salivary glands isolated from each successive larval stage. A gradual but steady decrease in the nuclear Dorsal signal was observed in the first instar to third instar stage nuclei of the ubiquitous control knockdown organisms. The salivary gland nuclei from the first instar larva of ubiquitous *dElys* depletion have the Dorsal signal inside the nucleus that is comparable with control depletion (Fig. 5*A*, *3rd vertical panel*). However, we observed an increase in nuclear levels of Dorsal in the second instar larval stage of *dElys*-depleted organisms, whereas control nuclei have only residual or no Dorsal signals (Fig. 5*A*, *4th vertical panel*). Importantly, the salivary glands from the third instar larval stage of ubiquitous *dElys* depletion show a prominent nuclear accumulation and a complementary decrease in the Dorsal signal inside the cytoplasm. But the control third instar salivary gland nuclei had no

Dorsal inside the nucleus, and the Dorsal levels remained restricted to cytoplasm only (Fig. 5*A*, *5th vertical panel*). Quantification of nuclear Dorsal signal intensities from control and *dElys*-depleted salivary gland nuclei further established that Dorsal starts to re-distribute in the nucleus during post-embryonic developmental stages upon *dElys* depletion (Fig. 5*B*). To further support this observation, we followed the expression of three Dorsal targets, namely *snail*, *twist*, and *sog*, which are key determinants of dorsoventral polarity in successive developmental stages. Under *dElys*-depleted conditions, the expression of *snail*, *twist*, and *sog* is high during the early embryonic stage, which diminished during the first instar larval stage after specifying dorsoventral polarity. But a resurrected expression of these key molecules was observed during the third instar stage when *dElys* was depleted. Under the control depletion condition, there is no significant expression observed during the late larval stages (Fig. 5*C*). Our results thus strongly suggest that *d*Elys plays an important role in regulating the Dorsal signaling during post-embryonic stages and its temporal sequestration in the cytoplasm.

We next asked whether this nuclear re-localization of Dorsal is specific to *dElys* depletion or a general consequence of a lack of properly-assembled nuclear pores. To check this, we investigated Dorsal localization in salivary gland nuclei from the knockdown of critical nucleoporins *nup160*, *nup133*, *nup107*, and *nup153*. Members of the Nup107 complex play a key regulatory role in post-mitotic and interphase NPCs assembly, although Nup153 is a critical molecule for interphase NPCs assembly only (46–48). RNAi-mediated depletion of *nup160* and *nup107* caused lethality at the first instar larval stage; however, when reared at 23 °C, organisms from these crosses could survive until third instar larva. The salivary gland nuclei from *nup160* and *nup107* depletion do not show significant accumulation of Dorsal inside the nucleus (nuclear/cytoplasmic Dorsal: control, 1.00 ± 0.05, and *nup160*^{GD}, 0.95 ± 0.02; *nup107*^{KK}: 1.05 ± 0.02) (Fig. 5*D*). When compared with control, *nup153* depletion shows no significant difference in Dorsal signals inside the nuclei. Only *nup133* depletion showed little accumulation of nuclear Dorsal, which is still significantly lower than *d*Elys (nuclear/cytoplasmic Dorsal: *nup153*^{TRiP}, 1.11 ± 0.03, and *nup133*^{KK}, 1.57 ± 0.10) (Fig. 5*D*). The knockdown of these nucleoporins suggests a drastic loss in their expression (Fig. S6, *B–E*). mAb414 staining of salivary gland nuclei indicated that removal of these other nucleoporins had induced NPC assembly defects (Fig. S7). Accordingly, the mRNA export was also perturbed that led to accumulation of mRNA inside the nucleus (nuclear mRNA: control, 1.00 ± 0.11; *dElys*^{KK}, 1.87 ± 0.23; *nup160*^{GD}, 3.68 ± 0.28; *nup107*^{KK}, 7.29 ± 0.59; and *nup153*^{TRiP}, 3.84 ± 0.28) (Fig. S8, *A* and *B*). Moreover, GFP–NLS import assay showed increased GFP–NLS signals in the cytoplasm suggesting that the import process is also affected (cytoplasmic/nuclear GFP–NLS: control, 1.00 ± 0.08; *dElys*^{KK}, 1.85 ± 0.07; *nup160*^{GD}, 2.32 ± 0.19; *nup107*^{KK}, 2.13 ± 0.15; and *nup133*^{KK}, 2.03 ± 0.08) (Fig. S8, *C* and *D*). Quantitation of nuclear intensities of the Dorsal signal demonstrates that the Dorsal signal inside the nucleus increased by ~5-fold upon *dElys* depletion, but the same remains largely unchanged upon depletion of other tested nucleoporins involved in NPC assem-
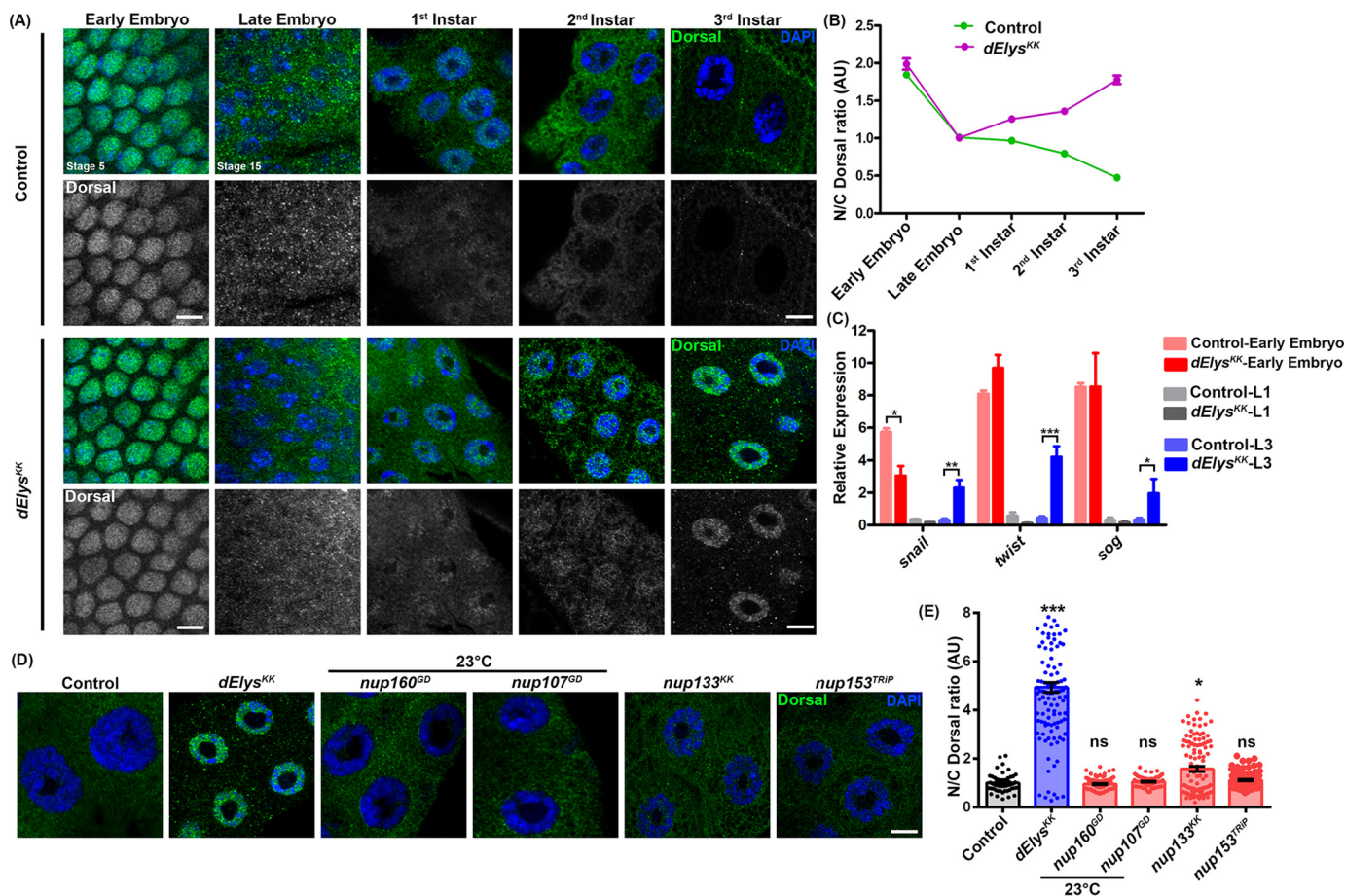
Figure 5. *d*Elys depletion re-distributes Dorsal in the nucleus during the larval stage and specific to *d*Elys. *A,* nuclear localization of Dorsal (*green*) assessed in control and *d*Elys depletion in each stage of development. The *1st two vertical panels* show early and late embryonic stages, and the *next three vertical panels* show each successive larval stage salivary glands. DNA is stained with DAPI. *Scale bar,* 5 μm. Early embryonic depletion was driven with *mat–α-tub–*GAL4. Control is WT flies crossed with the *mat–α-tub–*GAL4 (for early embryos) and ubiquitous *Act*5C–GAL4 (for late embryo and later developmental stages) driver, respectively. Stages of embryonic development are mentioned. *B,* quantitation of nuclear/cytoplasmic intensity ratio of Dorsal measured through developmental stages of *Drosophila* and plotted for each stage showing the distribution of Dorsal in embryos and salivary gland cells. Data represent at least three independent experiments. Data are represented from at least three independent experiments. *Error bar* represents S.E. *C,* Dorsal target genes *snail, twist,* and *sog* expression was analyzed in successive developmental stages by quantitative-PCR. The *red bar* represents analysis in whole early embryos; the *gray bar* represents analysis in head complex tissues of the first instar larva, and the *blue bar* represents analysis in head complex tissues of third instar larva. Control and *d*Elys depletion graphs are mentioned with *different shades* in the image. Data are represented from at least three independent experiments. The *error bar* represents the standard deviation. *** represents $p < 0.0001$, ** represents $p < 0.001$, and * represents $p < 0.05$. *D,* Dorsal nuclear localization assessed in control and nucleoporin knockdown third instar larval salivary glands (ubiquitous *Act*5C–GAL4 driven). DNA is stained with DAPI. *Scale bar,* 5 μm. *Control* is WT flies crossed with the *Act*5C–GAL4 driver. RNAi-mediated knockdown of Nup160[GD] and Nup107[GD] was carried out at 23 °C to obtain third instar larva. *E,* quantitation of nuclear/cytoplasmic intensity ratio of Dorsal in control and nucleoporins knockdown salivary gland nuclei (ubiquitous *Act*5C–GAL4 driven). Data are represented from at least three independent experiments. At least 45 nuclei were analyzed from 7 to 8 pairs of salivary glands. Statistical significance derived from one-way ANOVA followed by Tukey's post hoc test. The *error bar* is S.E. *** represents $p < 0.0001$, and * represents $p < 0.05$; *ns* is nonsignificant.

bly (Fig. 5E). We suggest that the resurrected residence of the Dorsal inside the nucleus is *d*Elys-specific and not the outcome of the absence of functional NPCs in the nuclear envelope.

dElys depletion-induced apoptosis is Dorsal-mediated

We next examined whether the apoptosis and the nuclear localization of Dorsal are independent consequences of *dElys* depletion. We have created a genetic combination of *dElys* depletion in the *dorsal* null background, but the embryos showed lethality at the early embryonic stage (~stage 2) and hence could not be used in any relevant study (Fig. S9A). Analysis of *dElys*-depleted or *dorsal* null organisms revealed increased apoptosis (Dcp-1 staining) by embryonic stage 11 as compared with control (Fig. S9B). Hence, we employed the combined knockdown of *dElys* and *dorsal* and analyzed the apoptotic response from co-depleted salivary glands. In control

depletion, Dorsal remained cytoplasmic, and no Dcp-1 staining was observed (Fig. 6, *A*, *1st horizontal panels, B,* and *C*). However, *dElys* depletion induced accumulation of Dorsal, and the enhanced punctate staining of Dcp-1 was observed (Fig. 6, *A*, *2nd horizontal panels, B,* and *C*). When *dElys* and *dorsal* were co-depleted, nuclear levels of Dorsal and punctate Dcp-1 staining both reduced significantly in salivary gland tissues (total Dorsal intensity: control, 1.00 ± 0.09; *dElys*[KK], 1.00 ± 0.07; *dElys*[KK]: *dorsal*[KK], 0.56 ± 0.03; and total Dcp-1 intensity: control, 1.00 ± 0.09; *dElys*[KK], 2.25 ± 0.08; *dElys*[KK]: *dorsal*[KK], 1.14 ± 0.05) (Fig. 6, *A*, *3rd horizontal panels, B,* and *C*).

We next examined whether apoptosis can be rescued by overexpressing *diap-1* (*diap-1*[OE]) in the *dElys* knockdown. As ubiquitous overexpression of *diap-1* is lethal, we used localized expression using salivary gland-specific drivers, *Fkh*-GAL4; *C-147*-GAL4. Salivary gland-specific *dElys* depletion elicited
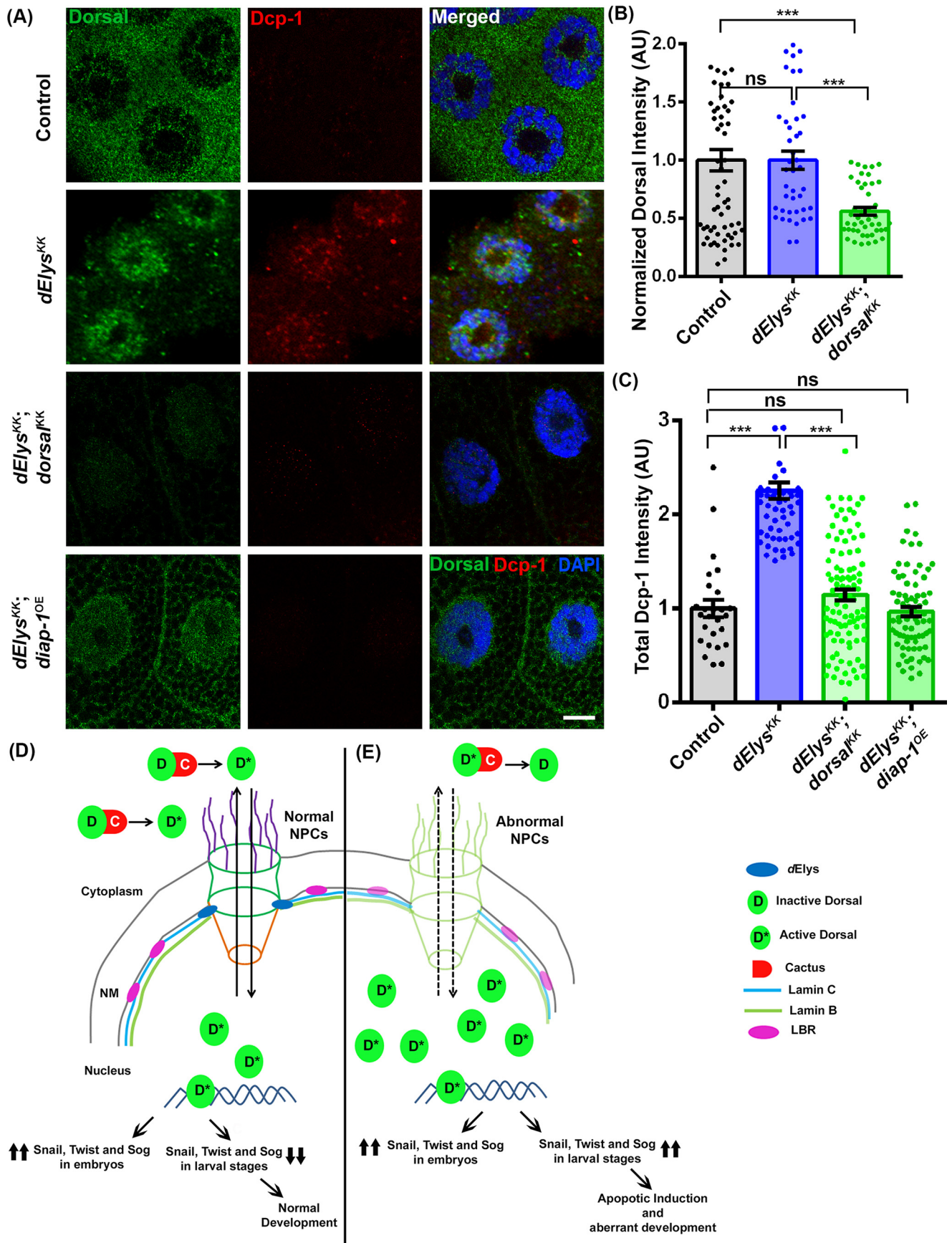
the Dcp-1 signal, but the *diap-1* overexpression in the *dElys* depletion background brings the Dcp-1 levels back to normal, subsiding the apoptotic response (total Dcp-1 intensity: *dElys^{KK}*, *diap-1^{OE}*, 0.96 ± 0.04) (Fig. 6, *A*, *4th horizontal panel*, and *C*). We further intended to rescue this phenotype in adult wings by using *nubbin*-GAL4; *Ubx*-GAL4 for expressing *diap-1* in *dElys* depletion background. We could partially rescue the apoptosis and wing phenotypes when *diap-1* is expressed in wing imaginal discs (Fig. S10*A*) of *dElys* knockdown (*dElys^{KK}*; *diap-1^{OE}*) organisms. The disc shape appears normal, and the Dcp-1 staining is reduced in the wing pouch region of the wing imaginal disc from *dElys^{KK}*; *diap-1^{OE}* organisms as compared with *dElys^{KK}* organisms (total Dcp-1 intensity in Wing imaginal discs: control, 1.00 ± 0.30, and *dElys^{KK}*, 6.42 ± 1.42; *dElys^{KK}*; *diap-1^{OE}*, 3.41 ± 0.42) (Fig. S10, *B* and *C*). The wings in adults arising from this genetic combination show improved morphology compared with *dElys* depletion (Fig. S10*D*). We attributed this partial rescue to the weak expression of *Ubx*-Gal4 in the wing-pouch area, which forms the major surface of wings. Together, our data strongly suggest that the induction of apoptosis upon *dElys* depletion is Dorsal-mediated, and the abundance of DIAP-1 counters the apoptotic phenotypes of *dElys* depletion.

Discussion

ELYS was found in stable association with the Nup107 complex of nuclear pores (6–8), and studies revealed that ELYS recruits Nup107 complex to the kinetochores and helps in regulation of Nup107 complex-mediated microtubule formation at the kinetochores (12, 49, 50). The biochemical characterization of AT-hook–like motif in the *Drosophila* ELYS ortholog (*dElys*) encoded by *CG14215* has echoed the view that positively-charged amino acid residues play an important role in the DNA binding (Fig. 1), similar to what has been observed with noncanonical AT-hook of *Drosophila* TAF-1 (25). The DNA-binding ability enables ELYS to initiates NPC assembly at a precise location and not at ectopic sites (11, 49, 51). The conserved localization of *dElys* to the nuclear rim in interphase also suggests a conserved function of *dElys* in *Drosophila*. However, unlike other characterized ELYS molecules (8, 12, 49, 50), *dElys* is absent from kinetochores and appears to envelop chromatin in mitosis (Fig. 1). The absence of *dElys* from the kinetochores provides a suitable explanation for the lack of *Drosophila*

Nup107 complex from the kinetochore during mitosis (23). Although *dElys* and Sec13 (a *d*Nup107 complex member) localize to the active chromatin regions (52), it remains to be elucidated whether they both interact physically.

The ubiquitous knockdown of *dElys*, induced developmental defects and lethality in *Drosophila* (Fig. 2) mirroring the defects observed in other organisms following the conserved function of ELYS molecules (6, 11, 53, 54). The *dElys* phenocopies nucleoporin functions of the ELYS molecule characterized in other organisms and is involved in nucleo-cytoplasmic transport regulation and NPC assembly and interacts with nuclear lamina proteins (Fig. 3) as reported in mammalian cell lines, *C. elegans* and *Xenopus* egg extract studies (6, 7, 9, 16, 28, 53), suggesting a conserved functional role in *Drosophila*. Nucleo-cytoplasmic transport defect observed in *dElys* depletion highlights its conserved role as a nucleoporin (7, 10, 55–57). We observed a conserved role for *dElys* in LBR recruitment to help organize the nuclear lamina, similar to what has been reported previously (17, 28). Importantly, we report the mislocalization of both lamin B and C from the nuclear lamina upon *dElys* depletion (Fig. 3). We attribute this mislocalization of lamin B and C to the loss of Ran from the nuclear periphery due to the probable reduction of Nup358 upon *dElys* loss. RanGTP helps in the dissociation of lamin from the lamin–importin α/β complex for incorporation into the nuclear lamina (58). Loss of Ran from the nucleus in *dElys* depletion might have hampered the dissociation of the lamin–importin α/β complex, in turn affecting nuclear lamina assembly in these nondividing salivary gland cells. This aspect of nuclear lamina assembly regulation by *d*Elys requires detailed investigation.

ELYS is known to initiate post-mitotic NPC assembly across different model organisms (6–11, 15, 49). Assembly of the NPCs, in turn, regulates the proper distribution of inner nuclear membrane proteins leading to correct nuclear architecture regulating proper nuclear transport (28, 59). So, NPC assembly, LBR localization, lamina assembly, and nuclear transport can be linked to nuclear pore–associated function of ELYS in *Drosophila*.

Dorsal (NF-κB) is a developmentally-regulated key transcription factor, and its nuclear localization and regulated activation of its downstream pathways are critical for normal development (34). The induction of the Dorsal signaling pathway

Figure 6. Dorsal depletion and *diap-1* overexpression can rescue *dElys* depletion apoptotic effects. *A*, apoptotic induction assessed in control (*1st horizontal panels*), *dElys* RNAi (*2nd horizontal panels*), *dElys*, *dorsal* co-depletion (ubiquitous *Act*5C–GAL4-driven, *3rd horizontal panels*), and *dElys* RNAi; *diap-1* overexpressed (salivary gland–specific expression, *4th horizontal panels*). Third instar larval salivary gland tissues were isolated from above genetic combination of organisms and stained with Dorsal (*green*) and Dcp-1 (*red*) antibodies. DNA is stained with DAPI. *Scale bar, 5* μm. *Control* is WT flies crossed with the *Act*5C–GAL4 driver as well as salivary gland–specific drivers. *B* and *C*, quantitation of signal intensity of Dorsal (*B*) and Dcp-1 (*C*) in the indicated samples. Data are derived from at least three independent experiments. At least 45 nuclei were analyzed from 7 to 8 pairs of salivary glands. Statistical significance was derived from one-way ANOVA followed by Tukey's post hoc test. *Error bars* represent S.E. *** represents $p < 0.0001$, and *ns* is nonsignificant. A theoretical model integrating the observations of the study is shown. *D*, under normal conditions, *d*Elys initiates postmitotic NPC assembly leading to functional nuclear pore in the nuclear membrane and normal organization of the nuclear lamina. Nuclear-cytoplasmic shuttling of Dorsal occurs conventionally leading to normal development. Dorsal is transported back to the cytoplasm through functional nuclear pores after completing the transcriptional regulation of key target genes in the nucleus. Inside cytoplasm, Dorsal is kept inactive by binding with Cactus, by certain post-translational modifications, or may be degraded. *E*, under *dElys*-depleted condition, nucleoporins and nuclear lamina components are mislocalized. The NPC assembly and functional nuclear pore formation are perturbed, and the nuclear lamina organization also is compromised. Dorsal translocates into the nucleus during early developmental stages, exits as normal, but during larval stage re-enters the nucleus due to the defective nucleo-cytoplasmic shuttling of certain post-translational regulators of Dorsal in the nucleus or loss of its independent interaction with *d*Elys. Resurrected Dorsal inside nucleus activates transcription of Dorsal target genes which rather remain shut during the post-embryonic stage. The mistimed transcription of developmentally regulated proteins may induce apoptosis resulting in lethality and developmental defects. Thus, the presence of *d*Elys is critical for Dorsal localization, growth *versus* apoptosis fate choice and to the conventional developmental program of the organism.

plays an important role in the growth and development of the organism (60, 61). The ectopic presence of Dorsal inside the nucleus of *dElys*-depleted salivary gland tissues (Fig. 4) is in direct contrast to the presence of Dorsal inside the nucleus only during early embryonic stages or a microbial infection. It is rather uncommon for Dorsal to be present inside the nucleus in later stages of *Drosophila* development and could suggest an uncharacteristic Dorsal pathway activation. The Dorsal present inside the *dElys*-depleted third instar salivary gland nuclei is active and transcribes growth-promoting target genes *snail*, *twist*, and *sog*. Expression of these genes is generally restricted to embryonic stages of development. Besides, the expression of pro-apoptotic genes *reaper* and *hid* is also induced (Fig. 4). The *snail*, *twist*, and *sog* genes are known to induce apoptosis when expressed in an unregulated manner (43, 44). In accordance, an increase in apoptosis is evident in *dElys*-depleted salivary gland tissues (Fig. 4). The two contrasting paradigms of gene expression can generate a developmental imbalance resulting in apoptosis by a hitherto unknown mechanism. Dorsal can induce apoptotic responses, and emerging ideas suggest that Dorsal, depending on cues, helps in growth *versus* apoptotic fate choices (62). Thus, *dElys* depletion can regulate effective nucleo-cytoplasmic transport of important transcriptional regulators to induce apoptosis. Importantly, no other nucleoporin tested in our study, when depleted, phenocopied the Dorsal accumulation inside the nucleus (Fig. 5). These results emphasize a strong pore-independent function for *d*Elys in Dorsal localization. Detailed analysis exploring the interactions between *d*Elys, Dorsal, and upstream players of the Dorsal pathway will shed more light on nuclear pore independent functions of *d*Elys. The apoptotic consequence of an aberrant Dorsal pathway activation seems to be a signature of *d*Elys nucleoporin in *Drosophila*. Nucleoporin depletion and apoptosis are not uncommon, and our observation aligns with the apoptosis induction in astrocytoma cells when *nup107* is depleted (63).

Our observation regarding the Dorsal pathway activation is in direct contrast to what is known for another nucleoporin *mbo* (Nup88) in *Drosophila*. The deletion of the *mbo* did not affect the general nuclear import/export and nuclear lamina assembly. Nup88 interacted feebly with Dorsal, but more importantly, nuclear levels of activated Dorsal were reduced in response to infection when Nup88 was deleted (64). Our observation can imply that in addition to genetic interaction, *d*Elys may possess a physical interaction with Dorsal or Cactus. Nup88, along with other nucleoporins like Nup62, Nup153, and Nup214, plays important roles in developmental pathways (65–67), but a detailed mechanistic understanding of selective nuclear translocation of activated signals are lacking. ELYS targets protein phosphatases to the nucleus, which can dephosphorylate and export molecules back to the cytoplasm (18). Structural and functional conservation of *d*Elys may suggest that *d*Elys perhaps regulates the localization of an orthologous phosphatase to control the nucleo-cytoplasmic shuttling of Dorsal in *Drosophila*. It is also very likely that through phosphatases, *dElys* may regulate the phosphorylation-mediated degradation of Cactus, resulting in the nuclear translocation of Dorsal. It will be of great interest to identify whether such a

phosphatase is involved in the shuttling process of Dorsal in *Drosophila*. Our results highlight the key difference between *d*Elys and other nucleoporins and affirm a role for *d*Elys in developmental signaling in addition to NPC and nuclear lamina organization.

NF-κB family transcription factors play a critical role in normal growth and development. Their dysregulation leads to cancer, chronic inflammatory disease, and developmental defects (68, 69). WntD, the product of Dorsal/Twist/Snail Signaling, is a feedback inhibitor of Dorsal signaling. WntD inhibits the nuclear translocation of Dorsal, thus inactivating expression of downstream targets (70, 71). Our report highlights that the novel role of the nucleoporin, *d*Elys, in Dorsal regulation during the later stages of development is an addition to the growing pool of reports for molecules involved in the regulation of Dorsal signaling. Unlike WntD, *d*Elys is a novel intracellular regulator of Dorsal signaling.

We suggest that *d*Elys levels help maintain a tight balance between pro-growth and pro-apoptotic responses to achieve normal growth and development in *Drosophila*. *d*Elys does regulate development and could contribute to normal growth in post-mitotic, nondividing cells by keeping the NF-κB trigger under control in a spatiotemporal manner (Fig. 6).

Our study thus provides an initial hint to a novel but yet-to-be-identified pathway that involves noncanonical AT-hook–like motifs containing *d*Elys to regulate the spatiotemporal distribution of Dorsal to ensures proper growth and development in *Drosophila*. Suppression of Dorsal signaling after the embryonic stage by *d*Elys is an added layer of regulation to ensure proper growth and development. Moreover, there may be additional signaling cascades that are perturbed by changes in *d*Elys levels, which require further elucidation.

Materials and methods

In silico analysis

An ortholog of ELYS in *Drosophila* was identified by using mouse ELYS as the reference sequence. PSI-BLAST with three iterations using mouse ELYS and its AT-hook motif sequence was used against the nonredundant protein database at NCBI with default parameters. ELYS orthologs in other organisms were identified by similar searches in the NCBI database. T-coffee, a multiple sequence alignment server, was used for alignment (72). The aligned sequence was then used for visualization in Jalview and highlighted with a Clustal X color scheme. The phylogenetic tree was inferred from this analysis using Jalview (73). Protein sequence motifs were identified using the SMART database for the representative sequence from each organism (74). IBS was used to draw a scaled protein illustration for each protein (75). Percentage identity was calculated against mouse ELYS as a reference for each ELYS-like molecule. Secondary structure for CG14215 was predicted using PSIPRED version 3.3, DisoPRED, and DomPRED (76). Predicted secondary structure for N-terminal and the central helical domain was compared with the experimentally-proven secondary structure of human and mouse ELYS (3). 3D structure of NTD of CG1425 was modeled using a Phyre2 algorithm and mouse ELYS NTD structure as a template (21).

Fly strains and genetics

All flies were reared at 25 °C on standard corn meal–yeast–agar medium. RNAi crosses were grown at 28 °C for better expression of GAL4. *nup160^GD* and *nup107^GD* crosses were grown at 23 °C to obtain third instar larva. The RNAi line (KK 103547) for *CG14215* was obtained from the VDRC. Other fly lines used in this study were obtained from the Bloomington *Drosophila* Stock Centre (BDSC) at Indiana University or VDRC. Controls used in this study are F1 progeny from Driver line crossed with W^1118 flies. Fly lines used in this study are mentioned in Table S1. All the combinations and recombinations are made with standard fly genetics. Tissue-specific knockdown of *dElys* was achieved by *Act5C–GAL4*, *Ey-GAL4*, *Wg-GAL4*, *Fkh-GAL4*, *mat–α-tub–GAL4* drivers obtained from BDSC. For maternal knockdown F1, virgin females from the cross of RNAi and *mat–α-tub–GAL4* was crossed with RNAi males, and early embryos were collected from this cross.

Cloning and transgenic fly generation

We obtained the clone LD14710 containing the full-length *CG14215*-coding sequence in the pBluescript SK(−) vector from *Drosophila* Genomics Resource Centre (DGRC). This clone was used as a template for cloning full-length *CG14215* into pTVW (Vector Laboratory, No. 1091), a fly transformation vector with gateway cassette, UASt promoter, and N-terminal EYFP tag as well as in pTW (Vector No. 1129) vector containing gateway cassette and UASt promoter (obtained from DGRC gateway-1 collection). Cloning was done using the Gateway cloning kit as per the manufacturer's instructions (Thermo Fisher Scientific). RNAi lines against *CG14215* were generated by cloning 503 base pairs from exon 7 of *CG14215* predicted using SnapDragon algorithm at the *Drosophila* RNAi screening center website (FlyRNAi.org), which do not have any predicted off-targets (77), and cloned into the gateway-based pVALIUM10 RNAi vector obtained from *Drosophila* RNAi screening center (TRiP). Transgenic flies were generated at the Fly Facility of the Centre for Cellular and Molecular Platforms at the National Center for Biological Sciences (C-CAMP-NCBS), Bangalore, India. Primers used in this study are mentioned in Table S2.

Drosophila S2 cell culture and transfections

Drosophila S2 cells were grown in Schneider's *Drosophila* medium (Gibco, Thermo Fisher Scientific) supplemented with 10% fetal bovine serum (Gibco, Thermo Fisher Scientific) and 50 units/ml penicillin, 50 units/ml streptomycin, and 25 μg/ml amphotericin B (Gibco, Thermo Fisher Scientific) at 25 °C in a CO$_2$-free incubator. Full-length *CG14215* was cloned in pAVW (Vector No. 1087) from DGRC. S2 cells were transfected at 50% confluency with Effectene transfection reagent (Qiagen). Cells were grown for 3 days post-transfection. S2 cells were arrested in metaphase of mitosis by the addition of 20 μM MG-132 (RTU solution, Sigma) for 2 h at 25 °C.

Antibody generation and Western blotting

The C-terminal 343 amino acids of CG14215, which is a unique and most antigenic and hydrophilic part, were amplified from the LD14710 clone and subcloned into pET28a(+) vector. Protein was expressed in *Escherichia coli* BL21 (DE3) cells, induced using 200 μM IPTG (Sigma), and incubated at 18 °C overnight. Cells were pelleted down, lysed in 100 mM NaH$_2$PO$_4$, 10 mM Tris-HCl buffer, pH 8.0, containing 8 M urea and 1% Triton X-100, 50 μg/ml lysozyme, and 1× protease inhibitor mixture (Roche Applied Science). The recombinant protein was purified over Ni-NTA beads and eluted with low pH at 4.5 in 100 mM NaH$_2$PO$_4$, 10 mM Tris-HCl buffer, pH 8.0, containing 8 M urea. Protein was dialyzed against 100 mM NaH$_2$PO$_4$, 10 mM Tris-HCl buffer, pH 8.0, containing a decreasing amount of urea up to 2 M. Protein was concentrated using a centrifugal concentrator of 30 kDa (Amersham Biosciences, GE Healthcare). Protein was flash-frozen in liquid nitrogen and stored at −80 °C. Polyclonal antibody against CG14215 was generated in the rabbit at Abgenex, Bhubaneswar, Odisha, India. Antibodies were affinity-purified over purified antigens chemically cross-linked to *N*-hydroxysuccinimidyl-Sepharose beads (Sigma) and eluted with low pH, neutralized, and dialyzed against PBS overnight at 4 °C. Antibody against full-length *d*Nup43 was also generated using an identical protocol.

Larval head complexes were dissected in cold PBS from third Instar larva and lysed in Laemmli buffer. A total of two equivalent head complexes were loaded in each well of the gel. *Drosophila* S2 cells were pelleted down and lysed in 50 mM Tris-HCl, pH 7.6, 150 mM NaCl, 1 mM MgCl$_2$, 1 mM EDTA, 10% glycerol, 0.4% sodium deoxycholate, 1% Triton X-100, 0.5% SDS, 1% Nonidet P-40, 2× Protease inhibitor cocktail (PIC) (modified from Ref. 78). 5 and 10 μg of total protein was resolved onto 8% SDS-PAGE and transferred to methanol-activated polyvinylidene difluoride membrane (Merck-Millipore). Polyclonal anti-*d*Elys antibody was used at 1:1000, and anti-Nup43 antibody (1:500), anti-Nup98 (1:2500), anti-lamin B (1:2500), anti-lamin C (1:2500), anti-mAb414 (1:5000), anti-Ran (1:5000), and anti-α-tubulin (1:5000) dilutions with overnight incubation at 4 °C were used. The horseradish peroxidase–coupled secondary antibody was used at 1:15,000 dilutions for the detection of proteins in Western blotting developed with SuperSignal West Pico chemiluminescent substrate (Pierce, Thermo Fisher Scientific).

Immunostaining

In vivo localization of *d*Elys was revealed by immunostaining of *Drosophila* embryos. *mat–α-tub–GAL4*-driven W^1118 and *dElys^KK*-staged syncytial blastoderm embryos were collected on apple juice agar plates for 1 h and aged to 2.5–3 h at 25 °C. Embryos were processed, as mentioned elsewhere (79, 80). Briefly, embryos were dechorionated in a 1:1 solution of sodium hypochlorite (∼4% w/v available chlorine) and water until appendages from 80% of embryos disappear. Embryos were washed thoroughly in embryo wash buffer containing 0.2% NaCl and 0.05% Triton X-100 and fixed with 4% formaldehyde in heptane for 45 min at room temperature. Embryos were then devitellinized in 100% methanol for 30 min at room temperature. Embryos were blocked in 5% neutralized goat serum (The Jackson Laboratory). Processed embryos were then used for immunostaining with the anti-*d*Elys antibody (1:1000), mAb414 (1:500, Bio-legend), and anti-Dorsal (1:20, 7A4,

DSHB). Embryos were mounted in Vectashield mounting medium (Vector Laboratories).

For immunostaining of *Drosophila* salivary glands, ubiquitous *Act5C–GAL4*-driven first, second, or third instar larvae were dissected in cold PBS for isolation of salivary glands. Glands were fixed in freshly prepared 4% formaldehyde for 30 min at room temperature and washed thoroughly with 0.2% PBST (PBS + 0.2% Triton X-100). Salivary glands were blocked with 5% neutralized goat serum (The Jackson Laboratory) and stained with the following: anti-*d*Elys (1:1000), anti-*d*Nup43 (1:250), and mAb414 (1:500, Bio-legend); anti-Ran (1:5000, BD Biosciences); anti-lamin Dm0 (1:1000, ADL67.10, DSHB, deposited by Prof. Paul A. Fisher, Stony Brook University (81)); anti-lamin C (1:2000, gift from Prof. Paul A. Fisher, Stony Brook University (81)); anti-LBR (1:500, gift from Prof. George Krohne, University of Wurzburg, Germany (82)); anti-Nup98 (1:1000, gift from Dr. Cordula Schulz, University of Georgia (83)); anti-TBP (1:200 (30)) for overnight at 4 °C and also probed with anti-Dorsal (1:20, 7A4, DSHB (34)), 1:50 for Dorsal antibody gift from Dr. Zeitlinger (Stowers Institute); and anti-Cactus (1:50, 3H12, DSHB (34)). For apoptotic induction, salivary glands were probed with an anti-cleaved-Dcp-1 antibody (1:100, Cell signaling technology, #9578 (38)). Eye and wing imaginal discs were dissected from third instar larva and processed as described above for probing of apoptotic induction with the Dcp-1 antibody. Secondary antibodies used were anti-rabbit Alexa Fluor 568 (1:800, Thermo Fisher Scientific), anti-mouse Alexa Fluor 488 (1:800, Thermo Fisher Scientific), anti-guinea pig FITC (1:400, Jackson laboratories), anti-mouse Cy5 (1:500, Jackson Laboratories). DNA was stained with DAPI (1:5000, Thermo Fisher Scientific). Salivary glands were mounted in Vectashield mounting medium (Vector Laboratories).

Drosophila S2 cells were immunostained by immobilizing on 0.25 mg/ml concanavalin A– coated coverslips for 2 h at 25 °C. MG-132–arrested cells were fixed by 100% methanol at −20 °C, blocked with 5% neutralized goat serum (The Jackson Laboratory), and immunostained anti-*d*Elys (1:1000), anti-α-tubulin (1:1000, DSHB), and anti-CID (1:1000, a gift from Prof. Steve Henikoff, Fred Hutchinson Cancer Research Center, Seattle, WA (22)). All the steps of immunostaining of S2 cells were followed as per Ref. 84.

All the samples were imaged on Carl Zeiss LSM 780 up-right confocal microscope equipped with a ×63/1.4 N.A. oil immersion lens. Super-resolution microscopy of anti-CID antibody-labeled EYFP–*d*Elys transfected cells was done with a Carl Zeiss LSM 800 Airyscan inverted microscope. Images were processed for super-resolution in the in-built mathematical algorithm of Zen.2 software of LSM 800 Airyscan. Images were processed with ImageJ (National Institutes of Health) or Fiji software and Adobe Photoshop CS6 (Adobe Corp.).

Intensity quantification

Average signal intensities for each molecule were measured by using Zen-2012 (Carl Zeiss, Image Analysis software) or Fiji software, and graphs were plotted with GraphPad software (Prism). For the quantification of Dorsal and GFP–NLS nuclear localization, five different regions of interest (ROI) were defined per nucleus and the cytoplasm around it. The average intensity

from each ROI was measured using Zen-2012 (Carl-Zeiss, Image Analysis software), and the mean of those intensities was taken per nucleus and cytoplasm around it. The ratio of the nucleus and cytoplasmic mean intensity was calculated for the final graph. Dcp-1 signal intensities were measured using five ROIs per cell, and the mean of that is used for the final graph. Nuclear rim localization of different molecules was calculated as average intensity per nucleus, including the nuclear rim. All the experiments were performed as at least three independent replicates.

Bright-field microscopy

For imaging of eye and wing phenotype of *dElys* knockdown flies, 3 days old flies were anesthetized with diethyl ether (Merck) and immobilized on sticky gum for proper orientation of *Drosophila* eye. At least 10 flies from each knockdown experiment were imaged from three independent experiments for each genotype. *Drosophila* eyes were imaged using Leica fluorescent stereomicroscope M205 FA using a ×123 magnification of particular equipment. For wing imaging in case of wing phenotypes with a *dElys* knockdown and *dElys^{KK}; diap-1^{OE}*, 3-day-old fly wings from each genotype were dissected and placed on a glass slide under a coverslip and imaged directly under Leica upright light microscope DM2500 with a ×10 magnification (85). At least 15 pairs of wings from each genotype were examined from three independent crosses.

Scanning EM (SEM)

Drosophila eyes from eye-specific knockdown of *dElys* were imaged using a scanning electron microscope for detailed analysis of eye structure perturbations. Three-day-old flies from each RNAi cross was processed as per Ref. 86. Briefly, flies were anesthetized and fixed with 2.5% glutaraldehyde in PBS for 2 h at 4 °C. Flies were washed thoroughly twice with PBS+ 4% sucrose. Flies were dehydrated through a graded ethanol series and were subjected to critical point drying. Samples were mounted on aluminum stubs with carbon-conductive tape. Flies were coated with gold particles in a sputter coating apparatus. Samples were imaged using a Carl Zeiss Gemini II FESEM microscope. At least 10 flies from each genotype were imaged from three independent experiments.

In vitro DNA binding experiment

To analyze the DNA-binding activity of AT-hook–like motifs of *d*Elys, we purified a fragment spanning all three AT-hook–like DNA-binding motifs by cloning the C-terminal 104 amino acids (1858–1961) from clone LD14710 into pET28a (+) vector. The His$_6$-tagged AT-hook motif fragment was purified by expressing in *E. coli* BL21 (DE3) cells. Protein was induced by 200 μM IPTG (Sigma) overnight at 18 °C. Cells were lysed in lysis buffer containing 50 mM Tris-HCl, pH 8.0, 150 mM NaCl, 20 mM imidazole, 1% Triton X-100, and 50 μg/ml lysozyme on ice. Protein was purified over Ni-NTA beads by eluting in 300 mM imidazole in 50 mM Tris-HCl, pH 8.0, 150 mM NaCl, 1 mM MgCl$_2$, and 0.5 mM EDTA. Protein was dialyzed overnight against dialysis buffer, 50 mM Tris-HCl, pH 8.0, 150 mM NaCl, 1 mM MgCl$_2$, and 0.5 mM EDTA.

For site-directed mutagenesis of arginine residues, we used Q5 site-directed mutagenesis kit (New England Biolabs) with primers

coding mutated nucleotides. Primers used for mutagenesis are mentioned in Table S2. The clone described above was used as a template for site-directed mutagenesis where conserved arginines were mutated to alanine as shown in Fig. S2. Mutations were confirmed using DNA sequencing (IISER-Bhopal sequencing facility). Clones were transformed into *E. coli* BL21 (DE3) cells, and proteins were purified as mentioned earlier.

In vitro DNA-binding experiment was performed by incubating the template that contains 50% AT richness and 90% AT richness with purified WT and mutant proteins. A known cytosolic protein that does not bind to DNA was used as a negative control. DNA binding experiment was performed in binding buffer containing 100 mM Tris, 500 mM KCl, 10 mM DTT, pH 7.5, for 30 min at room temperature and analyzed onto a 0.8% agarose gel and detected by a UV transilluminator (UVP). Purified DNA used for the binding experiment is 5 nM, and the total purified protein was used at 0.5 μM concentrations. EMSA was performed by using the Lightshift Chemiluminescent EMSA kit (Pierce, Thermo Fisher Scientific) by using *Sdic* DNA oligonucleotides as described previously (25).

Total mRNA fluorescence in situ hybridization (mRNA-FISH)

Total mRNA-FISH was performed as per Ref. 87, with some modifications. Salivary glands from third instar larvae were dissected and fixed in 4% paraformaldehyde for 20 min at room temperature followed by the second fixation in 100% methanol for 10 min at 4 °C. Tissues were dehydrated in graded ethanol series for 5 min each. Cy3-labeled poly(dT) oligonucleotides (IDT) were denatured in hybridization buffer containing 50% formamide, 2× SSC (saline sodium citrate), 10% dextran sulfate, and 0.05% BSA at 70 °C for 5 min. Denatured poly(dT)–Cy3 was added at 0.1 pmol/μl concentration to the fixed tissue and incubated overnight at 37 °C for hybridization. Tissues were washed in 2× SSC twice. DAPI was added for staining DNA and mounted in Vectashield. Tissues were imaged using the LSM 780 laser-scanning confocal microscope.

Quantitative-PCR

Total RNA was isolated from control and *d*Elys knockdown with either *mat–α-tub*–GAL4-driven early embryos or ubiquitous *Act5C–GAL4*-driven first and third instar larval head complex using total tissue RNA isolation kit (Favorgen Biotech). One μg of total RNA was used to synthesize cDNA using iScript cDNA synthesis (Bio-Rad). cDNA was diluted five times, and 1 μl of cDNA from each genotype was used as a template. Semi-quantitative PCR was done using gene-specific primers and *RpL49* as control. Real-time PCR on the same cDNA was done in Lightcycler 480 (Roche Applied Science) at standard cycling conditions and probed with SYBR Green (Bio-Rad) in real-time using *dElys* and actin RT primers. Quantification of each reaction was done by calculating ΔC_T values. ΔC_T was normalized against C_T values of *actin*. The graph was plotted as fold change in *d*Elys expression using GraphPad software (Prism). Primers used in quantitative PCR are mentioned in Table S2.

Hatching rate analysis

Embryos from control and *dElys* RNAi-driven with *mat–α-tub*–GAL4 were collected for 5 h and aged at 28 °C for 48 h after counting the total number of embryos. After 48 h, the number of intact, unhatched embryos were counted manually under the stereoscope. The percentage of unhatched embryos was determined by the ratio of unhatched embryos to the total number of embryos collected. Each experiment was performed with at least three independent replicates.

References

1. Kimura, N., Takizawa, M., Okita, K., Natori, O., Igarashi, K., Ueno, M., Nakashima, K., Nobuhisa, I., and Taga, T. (2002) Identification of a novel transcription factor, ELYS, expressed predominantly in mouse foetal haematopoietic tissues. *Genes Cells* **7,** 435–446 CrossRef Medline
2. Okita, K., Nobuhisa, I., Takizawa, M., Ueno, M., Kimura, N., and Taga, T. (2003) Genomic organization and characterization of the mouse ELYS gene. *Biochem. Biophys. Res. Commun.* **305,** 327–332 CrossRef Medline
3. Bilokapic, S., and Schwartz, T. U. (2013) Structural and functional studies of the 252-kDa nucleoporin ELYS reveal distinct roles for its three tethered domains. *Structure* **21,** 572–580 CrossRef Medline
4. Hetzer, M. W. (2010) The nuclear envelope. *Cold Spring Harb. Perspect. Biol.* **2,** a000539 CrossRef Medline
5. Hoelz, A., Debler, E. W., and Blobel, G. (2011) The structure of the nuclear pore complex. *Annu. Rev. Biochem.* **80,** 613–643 CrossRef Medline
6. Franz, C., Walczak, R., Yavuz, S., Santarella, R., Gentzel, M., Askjaer, P., Galy, V., Hetzer, M., Mattaj, I. W., and Antonin, W. (2007) MEL-28/ELYS is required for the recruitment of nucleoporins to chromatin and postmitotic nuclear pore complex assembly. *EMBO Rep.* **8,** 165–172 CrossRef Medline
7. Galy, V., Askjaer, P., Franz, C., López-Iglesias, C., and Mattaj, I. W. (2006) MEL-28, a novel nuclear-envelope and kinetochore protein essential for zygotic nuclear-envelope assembly in *C. elegans*. *Curr. Biol.* **16,** 1748–1756 CrossRef Medline
8. Rasala, B. A., Orjalo, A. V., Shen, Z., Briggs, S., and Forbes, D. J. (2006) ELYS is a dual nucleoporin/kinetochore protein required for nuclear pore assembly and proper cell division. *Proc. Natl. Acad. Sci. U.S.A.* **103,** 17801–17806 CrossRef Medline
9. Rasala, B. A., Ramos, C., Harel, A., and Forbes, D. J. (2008) Capture of AT-rich chromatin by ELYS recruits POM121 and NDC1 to initiate nuclear pore assembly. *Mol. Biol. Cell* **19,** 3982–3996 CrossRef Medline

10. Fernandez, A. G., and Piano, F. (2006) MEL-28 is downstream of the Ran cycle and is required for nuclear-envelope function and chromatin maintenance. *Curr. Biol.* **16,** 1757–1763 CrossRef Medline

11. Gómez-Saldivar, G., Fernandez, A., Hirano, Y., Mauro, M., Lai, A., Ayuso, C., Haraguchi, T., Hiraoka, Y., Piano, F., and Askjaer, P. (2016) Identification of conserved MEL-28/ELYS domains with essential roles in nuclear assembly and chromosome segregation. *PLoS Genet.* **12,** e1006131 CrossRef Medline

12. Yokoyama, H., Koch, B., Walczak, R., Ciray-Duygu, F., González-Sanchez, J. C., Devos, D. P., Mattaj, I. W., and Gruss, O. J. (2014) The nucleoporin MEL-28 promotes RanGTP-dependent γ-tubulin recruitment and microtubule nucleation in mitotic spindle formation. *Nat. Commun.* **5,** 3270 CrossRef Medline

13. Okita, K., Kiyonari, H., Nobuhisa, I., Kimura, N., Aizawa, S., and Taga, T. (2004) Targeted disruption of the mouse ELYS gene results in embryonic death at peri-implantation development. *Genes Cells* **9,** 1083–1091 CrossRef Medline

14. Gao, N., Davuluri, G., Gong, W., Seiler, C., Lorent, K., Furth, E. E., Kaestner, K. H., and Pack, M. (2011) The nuclear pore complex protein Elys is required for genome stability in mouse intestinal epithelial progenitor cells. *Gastroenterology* **140,** 1547–1555.e10 CrossRef Medline

15. Davuluri, G., Gong, W., Yusuff, S., Lorent, K., Muthumani, M., Dolan, A. C., and Pack, M. (2008) Mutation of the zebrafish nucleoporin elys sensitizes tissue progenitors to replication stress. *PLoS Genet.* **4,** e1000240 CrossRef Medline

16. de Jong-Curtain, T. A., Parslow, A. C., Trotter, A. J., Hall, N. E., Verkade, H., Tabone, T., Christie, E. L., Crowhurst, M. O., Layton, J. E., Shepherd, I. T., Nixon, S. J., Parton, R. G., Zon, L. I., Stainier, D. Y., Lieschke, G. J., and Heath, J. K. (2009) Abnormal nuclear pore formation triggers apoptosis in the intestinal epithelium of elys-deficient zebrafish. *Gastroenterology* **136,** 902–911 CrossRef Medline

17. Mimura, Y., Takagi, M., Clever, M., and Imamoto, N. (2016) ELYS regulates the localization of LBR by modulating its phosphorylation state. *J. Cell Sci.* **129,** 4200–4212 CrossRef Medline

18. Hattersley, N., Cheerambathur, D., Moyle, M., Stefanutti, M., Richardson, A., Lee, K. Y., Dumont, J., Oegema, K., and Desai, A. (2016) A nucleoporin docks protein phosphatase 1 to direct meiotic chromosome segregation and nuclear assembly. *Dev. Cell* **38,** 463–477 CrossRef Medline

19. Ilyin, A. A., Ryazansky, S. S., Doronin, S. A., Olenkina, O. M., Mikhaleva, E. A., Yakushev, E. Y., Abramov, Y. A., Belyakin, S. N., Ivankin, A. V., Pindyurin, A. V., Gvozdev, V. A., Klenov, M. S., and Shevelyov, Y. Y. (2017) Piwi interacts with chromatin at nuclear pores and promiscuously binds nuclear transcripts in *Drosophila* ovarian somatic cells. *Nucleic Acids Res.* **45,** 7666–7680 CrossRef Medline

20. Pascual-Garcia, P., Debo, B., Aleman, J. R., Talamas, J. A., Lan, Y., Nguyen, N. H., Won, K. J., and Capelson, M. (2017) Metazoan nuclear pores provide a scaffold for poised genes and mediate induced enhancer-promoter contacts. *Mol. Cell* **66,** 63–76.e6 CrossRef Medline

21. Kelley, L. A., Mezulis, S., Yates, C. M., Wass, M. N., and Sternberg, M. J. (2015) The Phyre2 web portal for protein modeling, prediction and analysis. *Nat. Protoc.* **10,** 845–858 CrossRef Medline

22. Vermaak, D., Hayden, H. S., and Henikoff, S. (2002) Centromere targeting element within the histone fold domain of Cid. *Mol. Cell. Biol.* **22,** 7553–7561 CrossRef Medline

23. Katsani, K. R., Karess, R. E., Dostatni, N., and Doye, V. (2008) *In vivo* dynamics of *Drosophila* nuclear envelope components. *Mol. Biol. Cell* **19,** 3652–3666 CrossRef Medline

24. Aravind, L., and Landsman, D. (1998) AT-hook motifs identified in a wide variety of DNA-binding proteins. *Nucleic Acids Res.* **26,** 4413–4421 CrossRef Medline

25. Metcalf, C. E., and Wassarman, D. A. (2006) DNA binding properties of TAF1 isoforms with two AT-hooks. *J. Biol. Chem.* **281,** 30015–30023 CrossRef Medline

26. Fatima, R. (2011) *Drosophila* Dynein intermediate chain gene, Dic61B, is required for spermatogenesis. *PLoS One* **6,** e27822 CrossRef Medline

27. Ni, J. Q., Zhou, R., Czech, B., Liu, L. P., Holderbaum, L., Yang-Zhou, D., Shim, H. S., Tao, R., Handler, D., Karpowicz, P., Binari, R., Booker, M., Brennecke, J., Perkins, L. A., Hannon, G. J., and Perrimon, N. (2011) A genome-scale shRNA resource for transgenic RNAi in *Drosophila*. *Nat. Methods* **8,** 405–407 CrossRef Medline

28. Clever, M., Funakoshi, T., Mimura, Y., Takagi, M., and Imamoto, N. (2012) The nucleoporin ELYS/Mel28 regulates nuclear envelope subdomain formation in HeLa cells. *Nucleus* **3,** 187–199 CrossRef Medline

29. Georgieva, S., Kirschner, D. B., Jagla, T., Nabirochkina, E., Hanke, S., Schenkel, H., de Lorenzo, C., Sinha, P., Jagla, K., Mechler, B., and Tora, L. (2000) Two novel *Drosophila* TAF(II)s have homology with human TAF(II)30 and are differentially regulated during development. *Mol. Cell. Biol.* **20,** 1639–1648 CrossRef Medline

30. Choudhury, S. D., Vs, A., Mushtaq, Z., and Kumar, V. (2017) Altered translational repression of an RNA-binding protein, Elav, by AOA2-causative Senataxin mutation. *Synapse* **71,** CrossRef Medline

31. Rushlow, C. A., Han, K., Manley, J. L., and Levine, M. (1989) The graded distribution of the dorsal morphogen is initiated by selective nuclear transport in *Drosophila*. *Cell* **59,** 1165–1177 CrossRef Medline

32. DeLotto, R., DeLotto, Y., Steward, R., and Lippincott-Schwartz, J. (2007) Nucleo-cytoplasmic shuttling mediates the dynamic maintenance of nuclear Dorsal levels during *Drosophila* embryogenesis. *Development* **134,** 4233–4241 CrossRef Medline

33. Belvin, M. P., Jin, Y., and Anderson, K. V. (1995) Cactus protein degradation mediates *Drosophila* dorsal-ventral signaling. *Genes Dev.* **9,** 783–793 CrossRef Medline

34. Whalen, A. M., and Steward, R. (1993) Dissociation of the dorsal–cactus complex and phosphorylation of the dorsal protein correlate with the nuclear localization of dorsal. *J. Cell Biol.* **123,** 523–534 CrossRef Medline

35. Kaltschmidt, B., Kaltschmidt, C., Hofmann, T. G., Hehner, S. P., Dröge, W., and Schmitz, M. L. (2000) The pro- or anti-apoptotic function of NF-κB is determined by the nature of the apoptotic stimulus. *Eur. J. Biochem.* **267,** 3828–3835 CrossRef Medline

36. Radhakrishnan, S. K., and Kamalakaran, S. (2006) Pro-apoptotic role of NF-κB: implications for cancer therapy. *Biochim. Biophys. Acta* **1766,** 53–62 CrossRef Medline

37. Ryan, K. M., Ernst, M. K., Rice, N. R., and Vousden, K. H. (2000) Role of NF-κB in p53-mediated programmed cell death. *Nature* **404,** 892–897 CrossRef Medline

38. DeVorkin, L., Go, N. E., Hou, Y. C., Moradian, A., Morin, G. B., and Gorski, S. M. (2014) The *Drosophila* effector caspase Dcp-1 regulates mitochondrial dynamics and autophagic flux via SesB. *J. Cell Biol.* **205,** 477–492 CrossRef Medline

39. McCall, K., and Steller, H. (1998) Requirement for DCP-1 caspase during *Drosophila* oogenesis. *Science* **279,** 230–234 CrossRef Medline

40. Song, Z., McCall, K., and Steller, H. (1997) DCP-1, a *Drosophila* cell death protease essential for development. *Science* **275,** 536–540 CrossRef Medline

41. Reeves, G. T., and Stathopoulos, A. (2009) Graded dorsal and differential gene regulation in the *Drosophila* embryo. *Cold Spring Harb. Perspect. Biol.* **1,** a000836 CrossRef Medline

42. Campbell, K., Lebreton, G., Franch-Marro, X., and Casanova, J. (2018) Differential roles of the *Drosophila* EMT-inducing transcription factors Snail and Serpent in driving primary tumour growth. *PLoS Genet.* **14,** e1007167 CrossRef Medline

43. Gullaud, M., Delanoue, R., and Silber, J. (2003) A *Drosophila* model to study the functions of TWIST orthologs in apoptosis and proliferation. *Cell Death Differ.* **10,** 641–651 CrossRef Medline

44. Lim, H. Y., and Tomlinson, A. (2006) Organization of the peripheral fly eye: the roles of Snail family transcription factors in peripheral retinal apoptosis. *Development* **133,** 3529–3537 CrossRef Medline

45. Neisch, A. L., Speck, O., Stronach, B., and Fehon, R. G. (2010) Rho1 regulates apoptosis via activation of the JNK signaling pathway at the plasma membrane. *J. Cell Biol.* **189,** 311–323 CrossRef Medline

46. Orjalo, A. V., Arnaoutov, A., Shen, Z., Boyarchuk, Y., Zeitlin, S. G., Fontoura, B., Briggs, S., Dasso, M., and Forbes, D. J. (2006) The Nup107-160 nucleoporin complex is required for correct bipolar spindle assembly. *Mol. Biol. Cell* **17,** 3806–3818 CrossRef Medline

47. Vollmer, B., Lorenz, M., Moreno-Andrés, D., Bodenhöfer, M., De Magistris, P., Astrinidis, S. A., Schooley, A., Flötenmeyer, M., Leptihn, S., and Antonin, W. (2015) Nup153 recruits the Nup107-160 complex to the

inner nuclear membrane for interphasic nuclear pore complex assembly. *Dev. Cell* **33,** 717–728 CrossRef Medline

48. Zuccolo, M., Alves, A., Galy, V., Bolhy, S., Formstecher, E., Racine, V., Sibarita, J. B., Fukagawa, T., Shiekhattar, R., Yen, T., and Doye, V. (2007) The human Nup107-160 nuclear pore subcomplex contributes to proper kinetochore functions. *EMBO J.* **26,** 1853–1864 CrossRef Medline

49. Gillespie, P. J., Khoudoli, G. A., Stewart, G., Swedlow, J. R., and Blow, J. J. (2007) ELYS/MEL-28 chromatin association coordinates nuclear pore complex assembly and replication licensing. *Curr. Biol.* **17,** 1657–1662 CrossRef Medline

50. Mishra, R. K., Chakraborty, P., Arnaoutov, A., Fontoura, B. M., and Dasso, M. (2010) The Nup107-160 complex and γ-TuRC regulate microtubule polymerization at kinetochores. *Nat. Cell Biol.* **12,** 164–169 CrossRef Medline

51. Sonneville, R., Craig, G., Labib, K., Gartner, A., and Blow, J. J. (2015) Both chromosome decondensation and condensation are dependent on DNA replication in *C. elegans* embryos. *Cell Rep.* **12,** 405–417 CrossRef Medline

52. Kuhn, T. M., Pascual-Garcia, P., Gozalo, A., Little, S. C., and Capelson, M. (2019) Chromatin targeting of nuclear pore proteins induces chromatin decondensation. *J. Cell Biol.* **218,** 2945–2961 CrossRef Medline

53. Cerveny, K. L., Cavodeassi, F., Turner, K. J., de Jong-Curtain, T. A., Heath, J. K., and Wilson, S. W. (2010) The zebrafish flotte lotte mutant reveals that the local retinal environment promotes the differentiation of proliferating precursors emerging from their stem cell niche. *Development* **137,** 2107–2115 CrossRef Medline

54. Lupu, F., Alves, A., Anderson, K., Doye, V., and Lacy, E. (2008) Nuclear pore composition regulates neural stem/progenitor cell differentiation in the mouse embryo. *Dev. Cell* **14,** 831–842 CrossRef Medline

55. Aitchison, J. D., Blobel, G., and Rout, M. P. (1995) Nup120p: a yeast nucleoporin required for NPC distribution and mRNA transport. *J. Cell Biol.* **131,** 1659–1675 CrossRef Medline

56. Emtage, J. L., Bucci, M., Watkins, J. L., and Wente, S. R. (1997) Defining the essential functional regions of the nucleoporin Nup145p. *J. Cell Sci.* **110,** 911–925 Medline

57. Fabre, E., and Hurt, E. (1997) Yeast genetics to dissect the nuclear pore complex and nucleo-cytoplasmic trafficking. *Annu. Rev. Genet.* **31,** 277–313 CrossRef Medline

58. Adam, S. A., Sengupta, K., and Goldman, R. D. (2008) Regulation of nuclear lamin polymerization by importin α. *J. Biol. Chem.* **283,** 8462–8468 CrossRef Medline

59. Hawryluk-Gara, L. A., Shibuya, E. K., and Wozniak, R. W. (2005) Vertebrate Nup53 interacts with the nuclear lamina and is required for the assembly of a Nup93-containing complex. *Mol. Biol. Cell* **16,** 2382–2394 CrossRef Medline

60. Espín-Palazón, R., and Traver, D. (2016) The NF-κB family: key players during embryonic development and HSC emergence. *Exp. Hematol.* **44,** 519–527 CrossRef Medline

61. Govind, S. (1999) Control of development and immunity by rel transcription factors in *Drosophila. Oncogene* **18,** 6875–6887 CrossRef Medline

62. Barkett, M., and Gilmore, T. D. (1999) Control of apoptosis by Rel/NF-κB transcription factors. *Oncogene* **18,** 6910–6924 CrossRef Medline

63. Banerjee, H. N., Gibbs, J., Jordan, T., and Blackshear, M. (2010) Depletion of a single nucleoporin, Nup107, induces apoptosis in eukaryotic cells. *Mol. Cell. Biochem.* **343,** 21–25 CrossRef Medline

64. Uv, A. E., Roth, P., Xylourgidis, N., Wickberg, A., Cantera, R., and Samakovlis, C. (2000) members only encodes a *Drosophila* nucleoporin required for rel protein import and immune response activation. *Genes Dev.* **14,** 1945–1957 Medline

65. Genenncher, B., Wirthmueller, L., Roth, C., Klenke, M., Ma, L., Sharon, A., and Wiermer, M. (2016) Nucleoporin-regulated MAP kinase signaling in immunity to a necrotrophic fungal pathogen. *Plant Physiol.* **172,** 1293–1305 CrossRef Medline

66. Xu, L., Kang, Y., Cöl, S., and Massagué, J. (2002) Smad2 nucleo-cytoplasmic shuttling by nucleoporins CAN/Nup214 and Nup153 feeds TGFβ signaling complexes in the cytoplasm and nucleus. *Mol. Cell* **10,** 271–282 CrossRef Medline

67. Yang, X., Gu, Q., Lin, L., Li, S., Zhong, S., Li, Q., and Cui, Z. (2015) Nucleoporin 62-like protein activates canonical Wnt signaling through facilitating the nuclear import of β-catenin in zebrafish. *Mol. Cell. Biol.* **35,** 1110–1124 CrossRef Medline

68. Park, M. H., and Hong, J. T. (2016) Roles of NF-κB in cancer and inflammatory diseases and their therapeutic approaches. *Cells* **5,** E15 CrossRef Medline

69. Xia, Y., Shen, S., and Verma, I. M. (2014) NF-κB, an active player in human cancers. *Cancer Immunol. Res.* **2,** 823–830 CrossRef Medline

70. Ganguly, A., Jiang, J., and Ip, Y. T. (2005) *Drosophila* WntD is a target and an inhibitor of the Dorsal/Twist/Snail network in the gastrulating embryo. *Development* **132,** 3419–3429 CrossRef Medline

71. Gordon, M. D., Dionne, M. S., Schneider, D. S., and Nusse, R. (2005) WntD is a feedback inhibitor of Dorsal/NF-κB in *Drosophila* development and immunity. *Nature* **437,** 746–749 CrossRef Medline

72. Notredame, C., Higgins, D. G., and Heringa, J. (2000) T-Coffee: a novel method for fast and accurate multiple sequence alignment. *J. Mol. Biol.* **302,** 205–217 CrossRef Medline

73. Waterhouse, A. M., Procter, J. B., Martin, D. M., Clamp, M., and Barton, G. J. (2009) Jalview Version 2–a multiple sequence alignment editor and analysis workbench. *Bioinformatics* **25,** 1189–1191 CrossRef Medline

74. Schultz, J., Milpetz, F., Bork, P., and Ponting, C. P. (1998) SMART, a simple modular architecture research tool: identification of signaling domains. *Proc. Natl. Acad. Sci. U.S.A.* **95,** 5857–5864 CrossRef Medline

75. Liu, W., Xie, Y., Ma, J., Luo, X., Nie, P., Zuo, Z., Lahrmann, U., Zhao, Q., Zheng, Y., Zhao, Y., Xue, Y., and Ren, J. (2015) IBS: an illustrator for the presentation and visualization of biological sequences. *Bioinformatics* **31,** 3359–3361 CrossRef Medline

76. Jones, D. T. (1999) Protein secondary structure prediction based on position-specific scoring matrices. *J. Mol. Biol.* **292,** 195–202 CrossRef Medline

77. Flockhart, I. T., Booker, M., Hu, Y., McElvany, B., Gilly, Q., Mathey-Prevot, B., Perrimon, N., and Mohr, S. E. (2012) FlyRNAi.org–the database of the *Drosophila* RNAi screening center: 2012 update. *Nucleic Acids res.* **40,** D715–D719 CrossRef Medline

78. Andlauer, T. F., Scholz-Kornehl, S., Tian, R., Kirchner, M., Babikir, H. A., Depner, H., Loll, B., Quentin, C., Gupta, V. K., Holt, M. G., Dipt, S., Cressy, M., Wahl, M. C., Fiala, A., Selbach, M., Schwarzel, M., and Sigrist, S. J. (2014) Drep-2 is a novel synaptic protein important for learning and memory. *Elife* **3,** CrossRef Medline

79. Harel, A., Zlotkin, E., Nainudel-Epszteyn, S., Feinstein, N., Fisher, P. A., and Gruenbaum, Y. (1989) Persistence of major nuclear envelope antigens in an envelope-like structure during mitosis in *Drosophila melanogaster* embryos. *J. Cell Sci.* **94,** 463–470 Medline

80. Johansen, K. M., and Johansen, J. (2004) Studying nuclear organization in embryos using antibody tools. *Methods Mol. Biol.* **247,** 215–234 CrossRef Medline

81. Riemer, D., Stuurman, N., Berrios, M., Hunter, C., Fisher, P. A., and Weber, K. (1995) Expression of *Drosophila* lamin C is developmentally regulated: analogies with vertebrate A-type lamins. *J. Cell Sci.* **108,** 3189–3198 Medline

82. Wagner, N., Weber, D., Seitz, S., and Krohne, G. (2004) The lamin B receptor of *Drosophila melanogaster. J. Cell Sci.* **117,** 2015–2028 CrossRef Medline

83. Parrott, B. B., Chiang, Y., Hudson, A., Sarkar, A., Guichet, A., and Schulz, C. (2011) Nucleoporin98–96 function is required for transit amplification divisions in the germ line of *Drosophila melanogaster. PLoS One* **6,** e25087 CrossRef Medline

84. Buster, D. W., Nye, J., Klebba, J. E., and Rogers, G. C. (2010) Preparation of *Drosophila* S2 cells for light microscopy. *J. Vis. Exp.* 1982 CrossRef Medline

85. Velentzas, P. D., Velentzas, A. D., Pantazi, A. D., Mpakou, V. E., Zervas, C. G., Papassideri, I. S., and Stravopodis, D. J. (2013) Proteasome, but not autophagy, disruption results in severe eye and wing dysmorphia: a subunit- and regulator-dependent process in *Drosophila. PloS one* **8,** e80530 CrossRef Medline

86. Wolff, T. (2011) Preparation of *Drosophila* eye specimens for scanning electron microscopy. *Cold Spring Harb. Protoc.* **2011,** 1383–1385 CrossRef Medline

87. Capelson, M., Liang, Y., Schulte, R., Mair, W., Wagner, U., and Hetzer, M. W. (2010) Chromatin-bound nuclear pore components regulate gene expression in higher eukaryotes. *Cell* **140,** 372–383 CrossRef Medline

ASBMB

J. Biol. Chem. (2020) 295(8) 2421–2437 **2437**